

PERIODICALLY DRIVEN
TWO-MODE
OPTICAL SYSTEMS

by

Ping Koy Lam
B.Sc., University of Auckland, 1990.

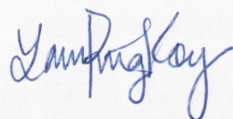
A thesis submitted for the degree of
Master of Science of the Australian National University.

April 1995

In memory of my father

Declaration

The contents of this thesis, except where indicated by references, are entirely my own work.

A handwritten signature in blue ink, appearing to read 'Lam Ping Koy', written in a cursive style.

Ping Koy Lam

April 1995

Acknowledgements

I sincerely thank my supervisor Dr. Craig Savage for his guidance, patience and support, without which it would have been impossible for me to begin or complete my Masters study. I would also like to thank Dr. John Love and Dr. Andrew Stevenson for giving me the valuable opportunity to work with them on their area of expertise.

I am privileged to have the acquaintance of the members of the Quantum Optics Group, particularly with Dr. Hans Bachor, Dr. David McClelland, Dr. Tim Ralph, Charles Harb and Joseph Hope. The many discussions with them and their frank opinions on my work have no doubt been very helpful. I also thank Dr. Alan Baxter for his efforts in helping me to overcome the many administrative obstacles throughout the course of my study.

I am grateful to my mother, my two brothers, my sister and Koon Chye Kua for their encouragement and moral support. Knowing that all of you are always there has helped me in getting through the hard times.

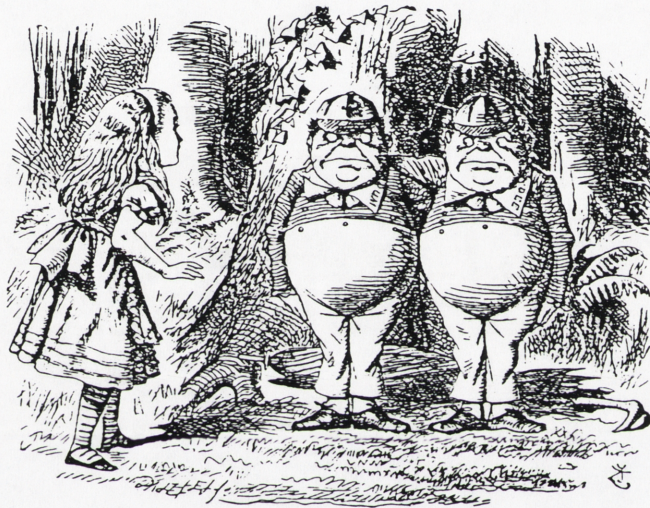
Finally, I thank my wife, Poh Ping, for her understanding; for her selfless decision of returning to student life with me and for her loving company.

Abstract

We consider a two-level atom driven by modulated light and find that complete population inversion can be induced by light without any resonant frequency component. This is in contrast to the familiar case of monochromatic driving in which complete population inversion is only possible with resonant light. This result concerns experimentally realizable systems and hence the effect of spontaneous emission is also considered. We also relate our work to other recent works on quantum double-well. Analogies with the suppression of quantum tunneling and with the low-frequency radiation generation are discussed.

By translating the results from the study of the two-level atom to the theory of optical waveguides, we introduce a new geometric representation for analysing the optical state of a single-mode optical coupler. We find that an optical coupler with out-of-phase index modulations can control and suppress the evanescent power transfer between cores. A new type of optical band-pass filter based on the modulated index coupler is proposed.

Alice's two-level system:



'I know what you're thinking about,' said Tweedledum; 'but it isn't so, nohow.'

'Contrariwise,' continued Tweedledee, 'if it was so, it might be; and if it were so, it would be; but as it isn't, it ain't. That's logic.'

Lewis Carroll [2].

Contents

1	Introduction	1
1.1	Overview and motivations	1
1.2	Thesis structure	2
2	Correlated Sideband Inversion	5
2.1	Overview	5
2.2	The generalized optical Bloch equations	6
2.3	Monochromatic light	7
2.4	Amplitude modulated light	9
2.5	Symmetrically detuned light	11
2.6	Phase modulated light	14
2.7	Phase modulation: Phase modulated rotating frame	18
2.8	Phase modulation: Sideband analysis	19
2.9	Effect of spontaneous emission	21
2.10	Outline of experiment	26
3	Suppression of Quantum Tunneling	28
3.1	Overview	28
3.2	2-level approximation of quantum double-well	29
3.3	Analogy with the two-level atom	30
3.4	Low-frequency radiation generation	32
4	Bloch representation of optical couplers	33
4.1	Overview	33
4.2	The Schrödinger equation and the scalar wave equation	34
4.3	Bloch representation for optical couplers	38

4.4	Uniform coupler	41
5	Modulated Index Coupler	44
5.1	Overview	44
5.2	The zero coupling condition	45
5.3	Numerical results	47
5.4	Bloch representation of the modulated index coupler	49
5.5	Square-wave longitudinal index coupler	51
5.6	Grating assisted coupler	53
5.7	Conclusion	55
6	Band-Pass Optical Coupler	57
6.1	Overview	57
6.2	Wavelength dependence of the modulated index coupler	58
6.3	Modulated index band-pass filter	60
6.4	Parameter variations	64
6.5	Conclusion	64
7	Conclusion	68

List of Figures

2.1	The atomic population inversion for monochromatic drivings	7
2.2	Maximum atomic population inversion versus laser detuning	9
2.3	Bloch sphere of detuned monochromatic driving	10
2.4	Fourier spectrum of amplitude modulation	11
2.5	Atomic population inversion of amplitude modulated driving	12
2.6	Symmetrically detuned driving arrangement	12
2.7	Atomic population inversion for single sideband driving	14
2.8	Atomic population inversion for symmetrically detuned sidebands	15
2.9	Fourier spectrum of phase modulation	15
2.10	Atomic population inversion for phase modulated light	17
2.11	The effective torque field for phase modulated driving	18
2.12	Effects of individual sidebands on the two-level atom I	19
2.13	Effects of individual sidebands on the two-level atom II	20
2.14	Monochromatic driving with spontaneous emission	22
2.15	Phase modulated driving with spontaneous emission	23
2.16	Monochromatic driving with spontaneous emission	24
2.17	Symmetrical sideband driving with spontaneous emission	25
2.18	Experimental setup for correlated sideband inversion demonstration . . .	26
4.1	The double wells of quantum mechanics and wave optics	37
4.2	The Bloch representation of an optical coupler	42
4.3	The Bloch representation of a uniform non-identical coupler	43
5.1	Schematic of a four-port modulated index coupler	46
5.2	Power transfer of a four-port modulated index coupler	48
5.3	Bloch representation of a four-port modulated index coupler	49

5.4	Bloch representation of the grating assisted coupler	52
5.5	Optical field vector evolution of the grating assisted coupler	54
5.6	Power transfer of the grating assisted coupler	55
6.1	Twin fibre band-pass filter geometry	58
6.2	Effective coupling constant versus wavelength	60
6.3	Spectral response of the four-port modulated index coupler	61
6.4	Spectral response of an identical core (unmodulated) coupler	61
6.5	Schematic of the modulated index band-pass filter	63
6.6	Effect of varying decay constant on band-pass filter response	65
6.7	Effect of varying device length on band-pass filter response	66

Chapter 1

Introduction

1.1 Overview and motivations

The studies of time-dependent two-level systems have been demonstrated to be rewarding in producing interesting breakthroughs in many areas of physics. A few of the notable greats are [10]:

Einstein

on the formulation of the rate equation using the A and B coefficients.

Rabi

on nuclear magnetic resonance and molecular beam techniques.

Bloch and Purcell

on magnetic fields in atomic nuclei and nuclear magnetic moments.

Townes, Basov and Prochorov

on the maser-laser principle.

There are many reasons for the successes in using the two-level models. They are simple systems to analyse, hence the complexity of a real physical problem can be reduced to a manageable simplicity. On the other hand, they contain rich enough characteristics to accurately describe many real physical systems. Unlike the simple harmonic oscillator, their non-linear properties also warrant their usefulness in modeling many non-linear

physical problems. The two-level models are therefore a good building block for the development of more complicated theories.

Yet another successful use of the two-level system is that it provides a simple explanation of the phenomenon of particle quantum tunneling in a potential double-well [10]. In 1991, Grossmann et. al. [24, 25] found that periodic perturbations of a potential double-well can control and, in particular, suppress quantum tunneling. Their discovery was based on results obtained by numerically solving the evolution of the wavefunction of a particle in a quartic potential well, taking into account the presence of all energy levels. It is therefore not surprising that shortly after the discovery, a simple two-level model is again used to demonstrate that such a phenomenon is also present without taking into consideration the other higher energy levels of a quartic potential well [27, 28]. This implies that the newly discovered phenomenon of quantum tunneling suppression, is actually an inherent property of the two-level system. Unfortunately, a physical explanation of the suppression of quantum tunneling was not manifested by both the quartic well and the two-level system analyses.

Because of the wide applicability of the two-level system, it is interesting to investigate similar periodic perturbations of other two-level systems modeling entirely different physical problems. The aim of the investigations is two-fold: they may provide new and more complete insights into the phenomenon of quantum tunneling suppression itself and may also reveal new applications of the phenomenon to different areas of physics.

In this thesis, we are primarily interested in periodic perturbations of two optical two-level systems: the interaction of light with a two-level atom and the optical field evolution in a single-mode optical coupler.

1.2 Thesis structure

Most of the results in this thesis are from the following papers:

1. P. K. Lam, A. J. Stevenson and J. D. Love, "Control and suppression of power transfer in couplers by periodic index modulation", *Electronics Letts.* **31**, 1233 (1995).

2. P. K. Lam, A. J. Stevenson and J. D. Love, "Coupling suppression by periodic index modulation in single-mode couplers", 19th Australian Conference on Optical Fibre Technology conference proceedings, 158 (1994).
3. P. K. Lam and C. M. Savage, "Complete atomic population inversion using correlated sidebands", Phys. Rev. A **50**, 3500 (1994).

The first part of this thesis, consisting of chapters 2 and 3, studies the properties of a two-level quantum system under the influence of periodic perturbation. We are mainly interested in the interaction of light with a two-level atom. We find that a two-level atom can achieve complete population inversion when driven by amplitude or phase modulated light with no resonant component. This is in contrast to the well known Rabi oscillation for monochromatic driving since only resonant Rabi oscillation can achieve complete population inversion. By making the two-level approximation of the double-well, we also show that the suppression of quantum tunneling is possible via sinusoidal perturbation. Equivalence between a two-level atom interacting with laser radiation and a particle in a double-well is established. This allows us to understand the suppression of quantum tunneling in terms of sideband excitations.

The second part of this thesis consist of chapters 4 through 6. In this part we apply the results obtained in the first part of the thesis to optical waveguide couplers. We show that many interesting applications of the concept of tunneling suppression are possible, physical devices like band-pass filters and switches can be built based on a mechanism analogous to the suppression of quantum tunneling. This is possible due to the close analogy between quantum mechanics and wave optics.

The contents of the individual chapters are as follow:

In chapter 2, we look at the interaction of light with a two-level atom using a semi-classical model and the Bloch equations. The phenomenon of using phase-locked non-resonant light to achieve complete atomic population inversion is discussed. We call this phenomenon "correlated sideband inversion". Two examples of correlated sideband inversion using amplitude and phase modulations of laser light are studied. Using a Bloch sphere picture, we are able to explain the occurrence of correlated sideband inversion. The study on the effect of spontaneous emission shows that correlated sideband inversion is not destroyed by spontaneous emission. We conclude the chapter by giving an outline of an optical experiment in which correlated sideband inversion can

potentially be observed.

In chapter 3, we review the work on the suppression of quantum tunneling. The mathematical equivalence between the model in chapter 2 and the suppression of quantum tunneling is shown. We show that using a suitable transformation between rotating frames, the suppression of quantum tunneling can also be explained by sideband interaction. We also relate the work in chapter 2 to work on low frequency generation [31].

In chapter 4, we begin by drawing the analogy between quantum mechanics and the wave optics. Because of the similarity between the Schrödinger equation and the scalar wave equation, we are able to establish a one-to-one correspondence between the parameters of the two models. It is found that the Bloch sphere used in analysing the interaction of light with a two-level atom can also be used to describe the evolution of optical fields in an optical coupler. An example of the use of the Bloch representation of an optical coupler is given.

In chapter 5, we make use of the formalism developed in chapter 4 to study the effect of periodically modulating the refractive indices of the cores of a coupler. It is found that an out-of-phase modulation can suppress power transfer between cores. We refer to this type of coupler as the modulated index coupler. The Bloch representation of the optical coupler is used to analyse this coupler as well as the grating assisted coupler. From the analysis, a zero coupling condition is obtained for the modulated index coupler. We also show that the criteria of complete power transfer in a grating assisted coupler can be obtained by simple geometric arguments using the Bloch representation.

In chapter 6, we make use of the results in chapter 5 to investigate the spectral response of a modulated index coupler. We show that with the addition of an absorptive medium along one of the cores of the modulated index coupler, an optical band-pass filter can be constructed. The design criteria of such a band-pass filter is discussed. It is found that the bandwidth and the suppression level of the band-pass filter is determined by the length of the coupler and the decay constant of the absorptive medium, respectively. Moreover, dynamic tunability of these parameters is achievable by using the electro-optic effect to induce the index modulation.

Finally, we give a brief summary of the important results obtained in this thesis in chapter 7.

Chapter 2

Correlated Sideband Inversion

2.1 Overview

Rabi oscillation of a two-level atom driven by monochromatic light is a central phenomenon in nonlinear optics [13]. And since it describes the dynamics of a driven two-level quantum system its significance extends beyond optics to a wide range of other physical systems [5, 6, 8]. In this chapter, we use the optical Bloch equations to analyse a two-level atom driven by modulated light. We are particularly interested in driving light which has no Fourier components at the atomic resonance frequency. A naive analysis might then suggest that complete atomic population inversion cannot occur. However we show that it does occur. This complete inversion is in contrast to the familiar case of monochromatic driving in which complete population inversion is only possible with resonant light. The requisite light has pair(s) of correlated sidebands without any resonant carrier. We refer to this kind of complete atomic population inversion as “correlated sideband inversion”.

Two experimentally accessible cases of correlated sideband inversion are: a single pair of phase locked (correlated) symmetrically detuned sidebands, and resonant light phase modulated so that all the power is in the modulation sidebands. Such light may be produced from a laser using acousto-optic and electro-optic modulators respectively [12].

We begin this chapter by reviewing the optical Bloch equations with monochromatic light before considering modulation. We then focus on the two previously described

cases of driving by a sideband pair and driving by phase modulated light. A Bloch sphere based physical interpretation of both cases is given. We conclude with a discussion of spontaneous emission and an outline of a possible non-linear optical experimental demonstration of correlated sideband inversion.

2.2 The generalized optical Bloch equations

In this section, we give a brief derivation of the optical Bloch equations from the interaction Hamiltonian and the Heisenberg equation. The electric dipole interaction of a single two-level atom with light has the following semi-classical Hamiltonian [13],

$$\hat{H} = \frac{1}{2}\hbar\omega_a\hat{\sigma}_z - d\hat{E}(t)\hat{\sigma}_x, \quad (2.1)$$

where d (taken to be real) is the atomic dipole moment in the direction of the electric field $\mathbf{E}(t)$, $\hat{\sigma}_x$ and $\hat{\sigma}_z$ are the Pauli spin operators and ω_a is the atomic transition frequency. The zero of energy for the atom is taken to be midway between the ground and excited states. We assumed that the quantum correlations between the field $E(t)$ and the atomic operators $\hat{\sigma}_i$ are insignificant, so that

$$\langle \hat{E}(t)\hat{\sigma}_i(t) \rangle = \langle \hat{E}(t) \rangle \langle \hat{\sigma}_i(t) \rangle. \quad (2.2)$$

This is known as the semi-classical approximation. The Heisenberg equations for the operators after the semi-classical approximation are,

$$\begin{aligned} \dot{\hat{\sigma}}_x &= -\omega_a\hat{\sigma}_y, \\ \dot{\hat{\sigma}}_y &= \omega_a\hat{\sigma}_x + 2\Omega_0\mathcal{E}(t)\hat{\sigma}_z, \\ \dot{\hat{\sigma}}_z &= -2\Omega_0\mathcal{E}(t)\hat{\sigma}_y, \end{aligned} \quad (2.3)$$

where the electric field has been factored into a constant amplitude E_0 and a time varying part, $E(t) = E_0\mathcal{E}(t)$. The quantity $\Omega_0 = dE_0/\hbar$, is called the resonant Rabi frequency. These Heisenberg equations are not very convenient to work with because they contain fast rotating terms at optical frequencies. We define rotating frame expectation values u , v , and w by,

$$\begin{aligned} u &= \cos\omega_1 t \langle \hat{\sigma}_x \rangle + \sin\omega_1 t \langle \hat{\sigma}_y \rangle, \\ v &= -\sin\omega_1 t \langle \hat{\sigma}_x \rangle + \cos\omega_1 t \langle \hat{\sigma}_y \rangle, \\ w &= \langle \hat{\sigma}_z \rangle, \end{aligned} \quad (2.4)$$

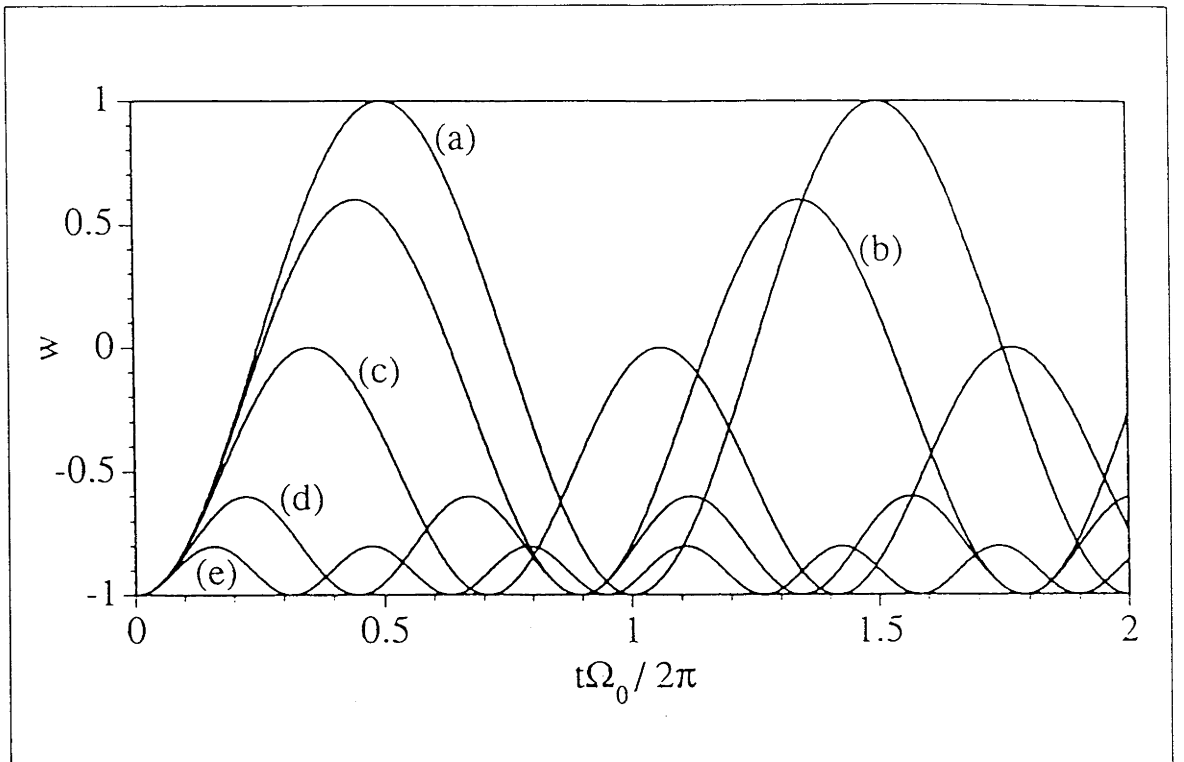


Figure 2.1: The atomic population inversion for monochromatic drivings. Atomic population inversion as a function of dimensionless time for detuning frequencies of $\delta/\Omega_0 =$ (a) 0.0 (resonant), (b) 0.5, (c) 1.0, (d) 2.0 and (e) 3.0.

where ω_l is normally the laser field frequency. Since the quantity of interest is the atomic inversion given by w , switching to this rotating frame will not alter the final results. The Heisenberg equations now become

$$\dot{u} = -\delta v + 2\Omega_0 \mathcal{E}(t) \sin \omega_l t w, \quad (2.5)$$

$$\dot{v} = \delta u + 2\Omega_0 \mathcal{E}(t) \cos \omega_l t w, \quad (2.6)$$

$$\dot{w} = -2\Omega_0 \mathcal{E}(t) [u \sin \omega_l t + v \cos \omega_l t], \quad (2.7)$$

where $\delta = \omega_a - \omega_l$ is the atom-field detuning frequency. Note that thus far the rotating wave approximation has not been made and no assumption has been made on the time dependence of the electric field. We call these equations the generalized optical Bloch equations.

2.3 Monochromatic light

An analytic solution to the optical Bloch equations can be found when the applied electric field is monochromatic with angular frequency ω_l , so that $\mathcal{E}(t) = \cos(\omega_l t)$.

In this case, u and $-v$ represent the in-phase and in-quadrature components of the atomic dipole moment, respectively. We make the rotating wave approximation to the dynamic equations of u, v , and w by neglecting any fast (optical frequency) rotating terms and thus obtain

$$\dot{u} = -\delta v, \quad (2.8)$$

$$\dot{v} = \delta u + \Omega_0 w, \quad (2.9)$$

$$\dot{w} = -\Omega_0 v. \quad (2.10)$$

These are the standard optical Bloch equations. Their solution is given by [13]

$$\begin{bmatrix} u(t) \\ v(t) \\ w(t) \end{bmatrix} = \begin{bmatrix} \frac{\Omega_0^2 + \delta^2 \cos \Omega t}{\Omega^2} & \frac{-\delta \sin \Omega t}{\Omega} & \frac{-\delta \Omega_0 (1 - \cos \Omega t)}{\Omega^2} \\ \frac{\delta \sin \Omega t}{\Omega} & \cos \Omega t & \frac{\Omega_0 \sin \Omega t}{\Omega} \\ \frac{-\delta \Omega_0 (1 - \cos \Omega t)}{\Omega^2} & \frac{-\Omega_0 \sin \Omega t}{\Omega} & \frac{\delta^2 + \Omega_0^2 \cos \Omega t}{\Omega^2} \end{bmatrix} \begin{bmatrix} u_0 \\ v_0 \\ w_0 \end{bmatrix}, \quad (2.11)$$

where u_0, v_0 and w_0 are the initial values, and Ω is the generalized Rabi frequency,

$$\Omega = \sqrt{\Omega_0^2 + \delta^2}. \quad (2.12)$$

When an initial ground state of $w(0) = -1$ is assumed, the atomic inversion is given by

$$w(t, \delta) = -\frac{\delta^2 + \Omega_0^2 \cos(\sqrt{\delta^2 + \Omega_0^2} t)}{\delta^2 + \Omega_0^2}. \quad (2.13)$$

This solution describes Rabi oscillation and Fig. 2.1 shows the effect of varying the detuning frequency on the atomic population inversion.

We observed that detuning increases the oscillation frequency and decreases the maximum inversion,

$$w_{max} = \frac{\Omega_0^2 - \delta^2}{\Omega_0^2 + \delta^2}. \quad (2.14)$$

So *non-resonant* ($\delta \neq 0$) *monochromatic light cannot yield complete atomic inversion* of $w_{max} = 1$. Fig (2.2) shows the Lorentzian profile of the maximum atomic inversion plotted as a function of laser detuning.

Introducing the Bloch vector $\rho = (u, v, w)$ allows the optical Bloch equations (2.8, 2.9, 2.10) to be written in the form of [13]

$$\dot{\rho} = \tau \times \rho, \quad (2.15)$$

where τ is dependent on the driving field. The dynamics of the Bloch vector is analogous to the Larmor precession of a magnetic dipole in a magnetic field. Hence we will

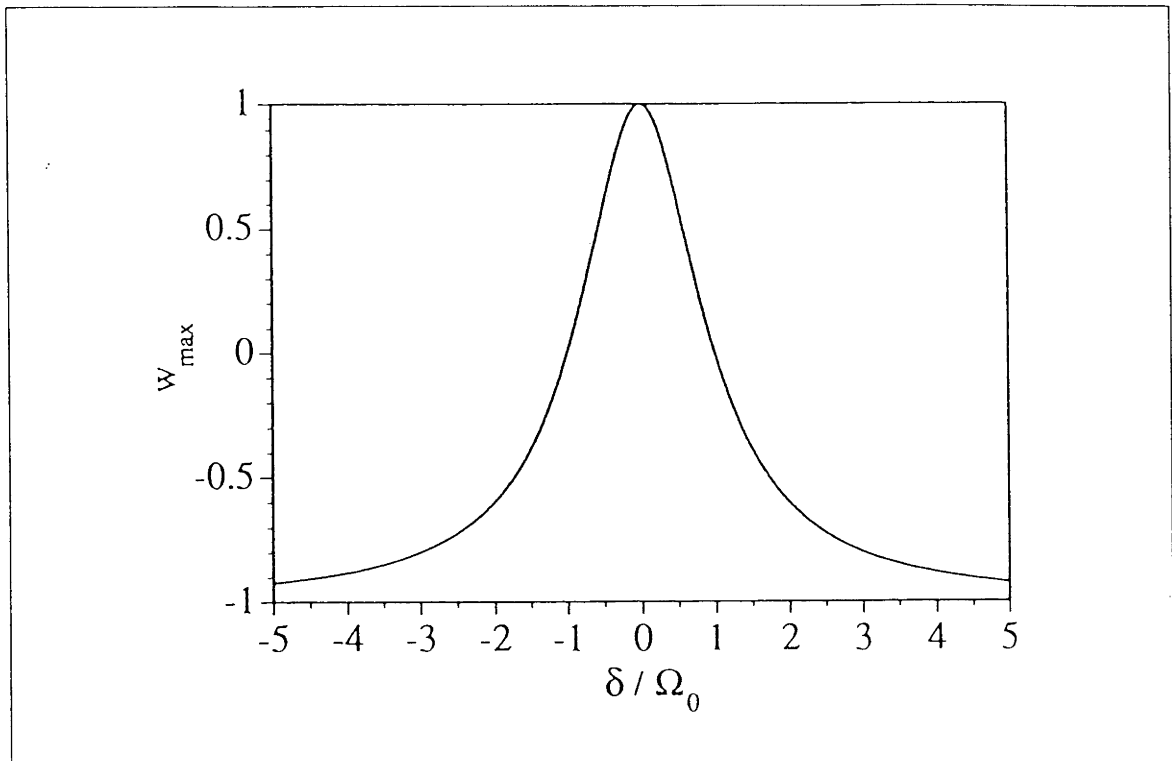


Figure 2.2: Maximum atomic population inversion versus laser detuning
The maximum achievable atomic population inversion versus detuning frequency gives a Lorentzian profile with a peak of $w_{\max} = 1$ at the resonant frequency.

refer to τ as the effective torque field. The modulus of ρ is conserved and has the value one. Hence the ρ dynamics occurs on a unit sphere, referred to as the “Bloch sphere”. This provides a useful picture for understanding driven two-level systems.

Driving with monochromatic detuned light corresponds to having an effective torque field of

$$\tau = (-\Omega_0, 0, \delta). \quad (2.16)$$

As shown by Fig 2.3, since the Bloch vector ρ makes a constant angle θ with τ , it rotates around the effective torque field, tracing out a small circle on the lower hemisphere of the Bloch sphere. Hence the optical vector does not intersect the “pole” $\rho = (0, 0, 1)$ corresponding to complete inversion.

2.4 Amplitude modulated light

In this section, we consider driving a two-level atom with amplitude modulated light. The amplitude modulation of light can be achieved, for example, by passing a monochro-

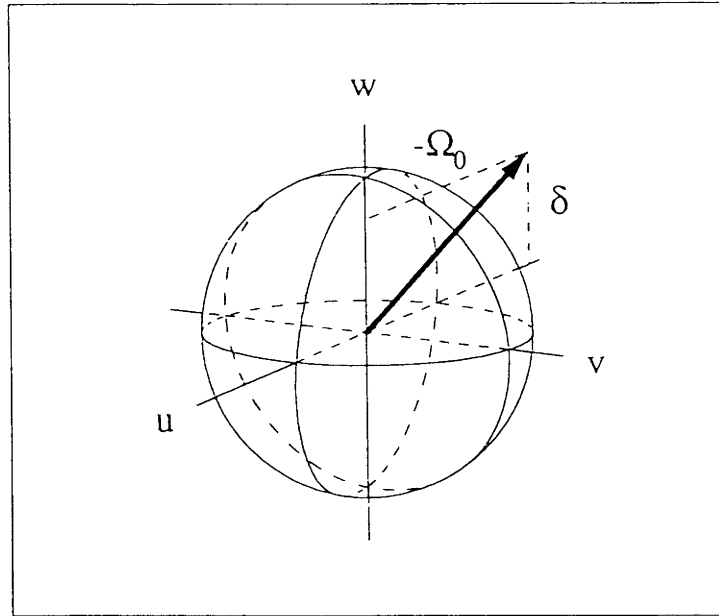


Figure 2.3: Bloch sphere of detuned monochromatic driving
The Bloch vector makes a constant angle $\theta = \tan^{-1}(-\Omega_0/\delta)$ with the effective torque field, assuming initial ground state $w = -1$.

matic light beam through an acousto-optic modulator. The general formula for amplitude modulation is given by [12]

$$\mathcal{E}(t) = [1 + Af(t)] \cos \omega_l t. \quad (2.17)$$

We restrict ourselves to consider only the case when $f(t) = \cos \omega_m t$. Hence ω_m is the amplitude modulation frequency and A the modulation index. The Fourier decomposition of the amplitude modulation gives a pair of sidebands detuned by the same amount of ω_m on either side of the carrier frequency as shown in Fig. 2.4.

The amplitude of the sidebands is given by $\frac{1}{2}A$ and hence their intensities depend on the modulation index. by substituting Eq. (2.17) into Eq. (2.5, 2.6, 2.7) we obtain,

$$\dot{u} = -\delta v, \quad (2.18)$$

$$\dot{v} = \delta u + \Omega_0[1 + A \cos \omega_m t]w, \quad (2.19)$$

$$\dot{w} = -\Omega_0[1 + A \cos \omega_m t]v. \quad (2.20)$$

Fig. 2.4 shows the atomic population inversion as a function of time for amplitude modulated driving. Since the amplitude modulation does not completely remove the carrier frequency, we observe that the atomic inversion is complete.

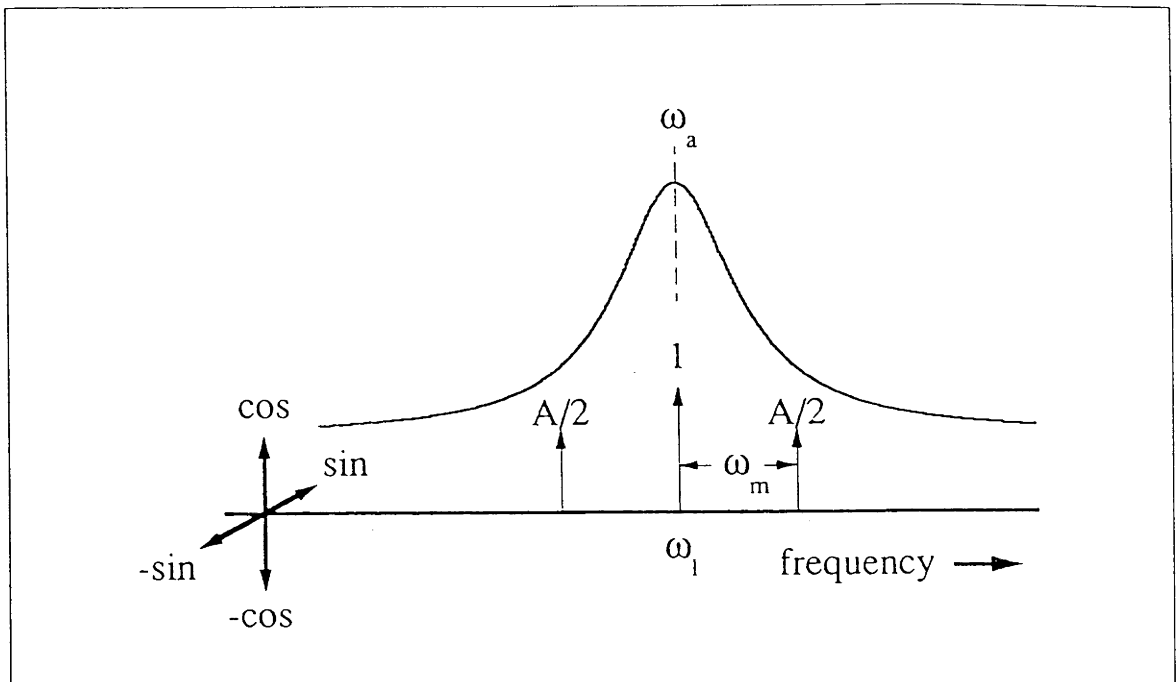


Figure 2.4: Fourier spectrum of amplitude modulation

The Lorentzian profile of maximum inversion is shown superimposed on the amplitude modulation Fourier spectrum. The length of the vectors show the relative strength of the carrier and sideband components.

2.5 Symmetrically detuned light

We now consider the case of driving by a pair of sidebands symmetrically detuned about resonance. We require that the two symmetrically detuned sidebands to be phase-locked to each other without which correlated sideband inversion will not occur. This requirement is experimentally achievable by amplitude modulating the laser light and then filtering off the lower sideband, say, leaving the carrier and the upper sideband phase locked. The carrier and the remaining sideband can then be chosen to have frequencies equally detuned from the atomic resonance by choosing $\omega_l = \omega_a - \omega_m/2$ as shown in Fig. 2.6. $\mathcal{E}(t)$ is then given by

$$\mathcal{E}(t) = \frac{1}{2} \left[\sin((\omega_a + \frac{1}{2}\omega_m)t) + \sin((\omega_a - \frac{1}{2}\omega_m)t) \right]. \quad (2.21)$$

The amplitude modulation index of $A = 2$ is chosen to ensure that the carrier and the sideband have equal intensities. The optical Bloch equations are given by,

$$\dot{u} = \Omega_0 \cos(\frac{1}{2}\omega_m t)w, \quad (2.22)$$

$$\dot{v} = 0, \quad (2.23)$$

$$\dot{w} = -\Omega_0 \cos(\frac{1}{2}\omega_m t)u, \quad (2.24)$$

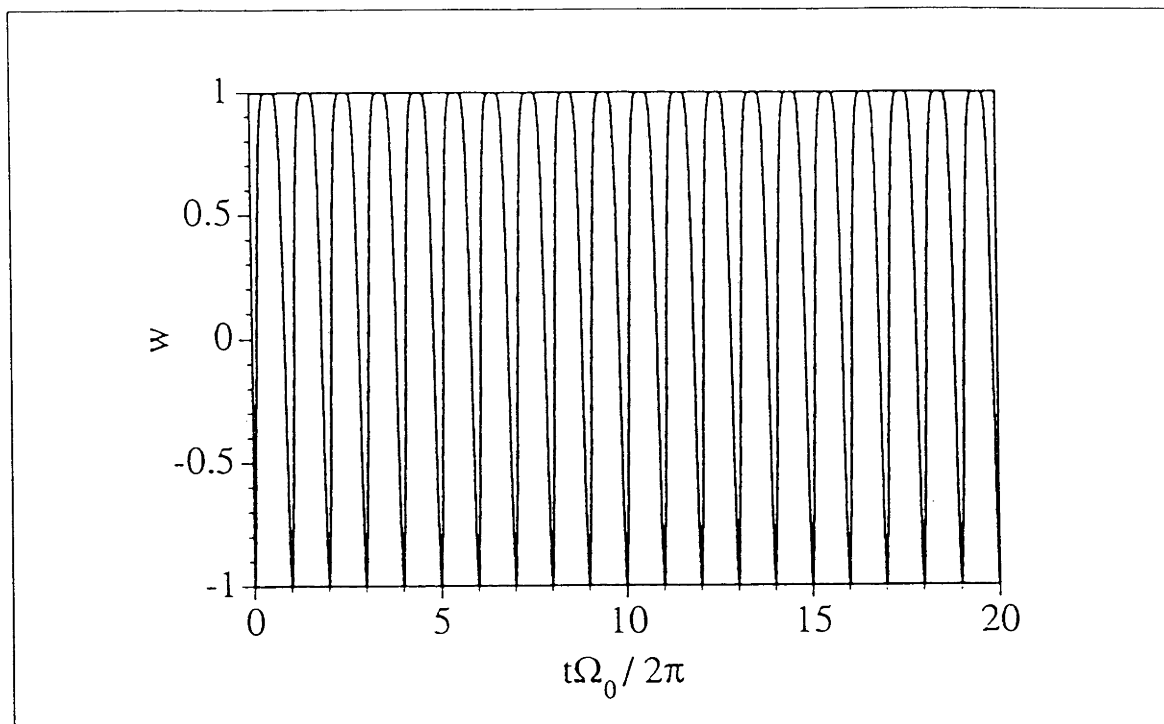


Figure 2.5: Atomic population inversion of amplitude modulated driving. Here the modulation index $A = 1$ and the laser light is resonant with the two-level atom $\delta = 0$. Note that the atomic inversion is dominated by the presence of the resonant component. Hence it oscillates at a frequency close to the resonant Rabi frequency. The effect of the sideband pair only slightly alters the shape of the oscillation.

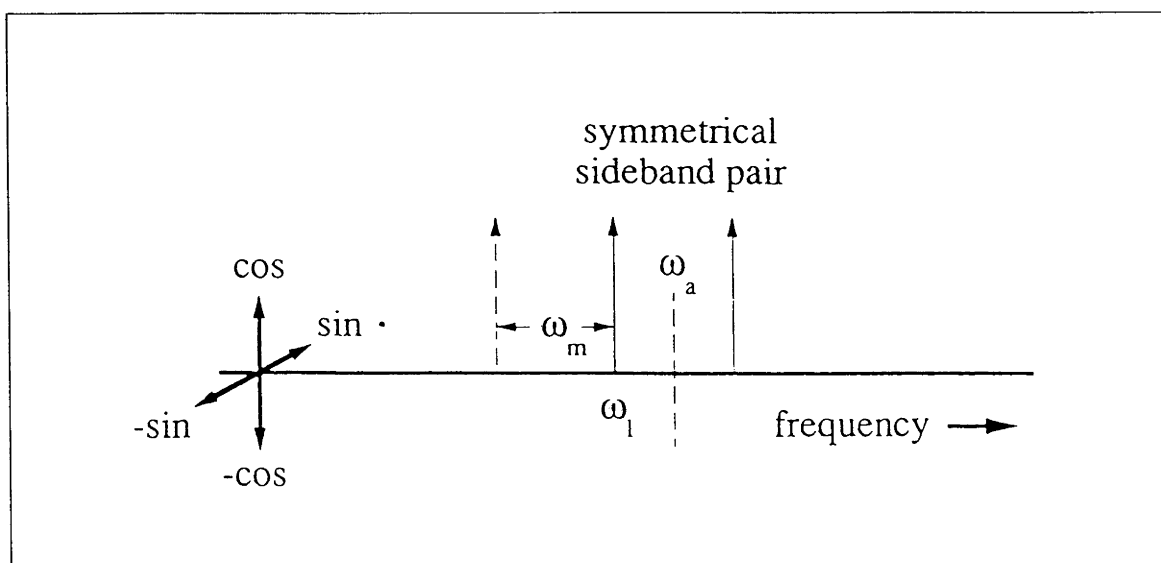


Figure 2.6: Symmetrically detuned driving arrangement. The amplitude modulation index $A = 2$, so that the carrier and the sidebands are equal in strength. The dashed vector shows the position of the lower sideband which is filtered off.

Since in this case the in-quadrature dipole moment is not coupled to the other atomic parameters, we can write the time evolution of the atomic inversion as a second order non-linear differential equation,

$$\ddot{w} + \omega_m \tan\left(\frac{1}{2}\omega_m t\right)\dot{w} + \Omega_0^2 \cos^2\left(\frac{1}{2}\omega_m t\right)w = 0. \quad (2.25)$$

This differential equation has the solution, assuming an initial ground state $w(0) = -1$, given by [7]

$$w = -\cos\left(\frac{2\Omega_0}{\omega_m} \sin\left(\frac{1}{2}\omega_m t\right)\right). \quad (2.26)$$

Eq. (2.26) shows that complete atomic inversion can be achieved provided the argument of the cosine can exceed π , that is provided that the inequality,

$$\pi \leq \frac{2\Omega_0}{\omega_m}, \quad (2.27)$$

is satisfied. This requires that the detuning be sufficiently small. This is our first example of correlated sideband inversion, for which complete atomic inversion is possible in the absence of resonant light. Note that linear combinations of the sideband and the carrier cannot reconstruct the resonant component because the Fourier components are orthogonal to each other. Hence this complete atomic population inversion is entirely due to the non-linear characteristic of the two-level atom driven by correlated sideband inversion. Fig. 2.8 and Fig. 2.5 compare such a case when $\omega_m = 0.50\Omega_0$ to normal monochromatic detuning.

This example of correlated sideband inversion can be understood using the Bloch sphere picture. For the pair of sidebands the effective torque field is,

$$\tau = (0, -\Omega_0 \cos(\omega_m t), 0), \quad (2.28)$$

which is a vector oscillating along the v -axis. For an initial ground state, the Bloch vector is thus confined to oscillate about $\rho = (0, 0, -1)$, in the v - w plane. When the inequality (2.27) is satisfied the oscillations swing through $\pm 180^\circ$ before τ changes direction, giving complete inversion $\rho = (0, 0, 1)$. Note that the relative phase of the two sidebands in Eq. (2.21) does not affect the induced inversion, as long as it remains constant.

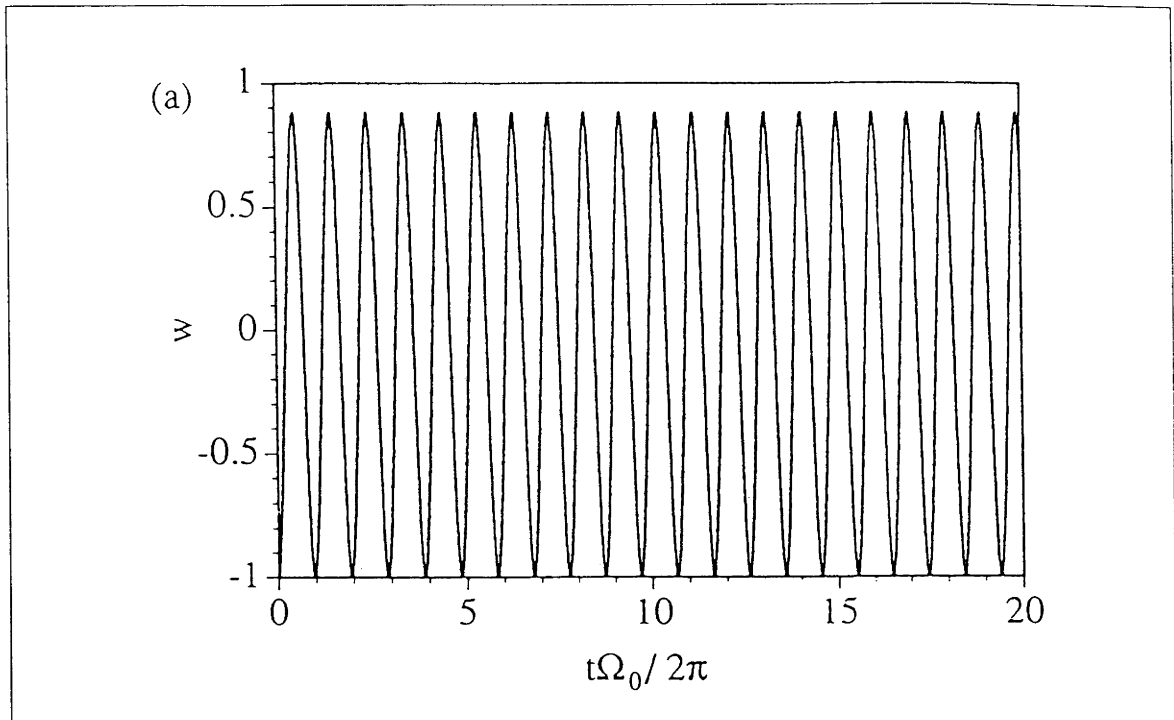


Figure 2.7: Atomic population inversion for single sideband driving
Atomic population inversion w as a function of dimensionless time for a two-level atom driven by a single sideband $\mathcal{E}(t) = \sin((\omega_a + \omega_m)t)$ with $\omega_m = 0.25\Omega_0$.

2.6 Phase modulated light

We next consider the phase modulated field,

$$\mathcal{E}(t) = \cos(\omega_a t + A \cos \omega_m t), \quad (2.29)$$

where A is the phase modulation index and $\omega_m \ll \omega_a$ is the modulation frequency. This is an interesting case since it can be realized by electro-optic modulation of a resonant laser. After making the rotating wave approximation on Eqs. (2.5, 2.6, 2.7) we find the optical Bloch equations,

$$\begin{aligned} \dot{u} &= -\Omega_0 \sin(A \cos \omega_m t) w, \\ \dot{v} &= \Omega_0 \cos(A \cos \omega_m t) w, \\ \dot{w} &= \Omega_0 [\sin(A \cos \omega_m t) u - \cos(A \cos \omega_m t) v]. \end{aligned} \quad (2.30)$$

The phase modulated light can be decomposed into its Fourier components [7]

$$\begin{aligned} \mathcal{E}(t) &= \cos(\omega_a t + A \cos \omega_m t) \\ &= J_0(A) \cos \omega_a t \end{aligned} \quad (2.31)$$

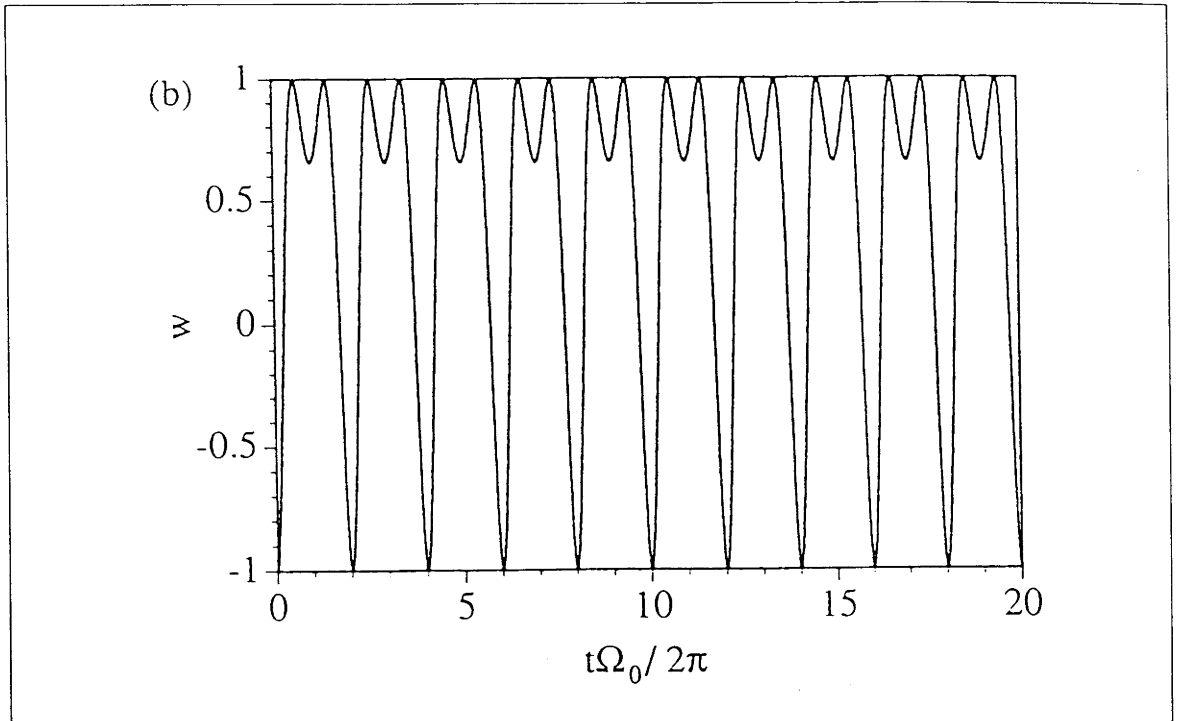


Figure 2.8: Atomic population inversion for symmetrically detuned sidebands
 Atomic population inversion w as a function of dimensionless time for a two-level atom driven by a pair of symmetrically detuned sidebands Eq. (2.21) with $\omega_m = 0.50\Omega_0$. The effective detuning of the carrier and upper sideband is $\pm 0.25\Omega_0$.

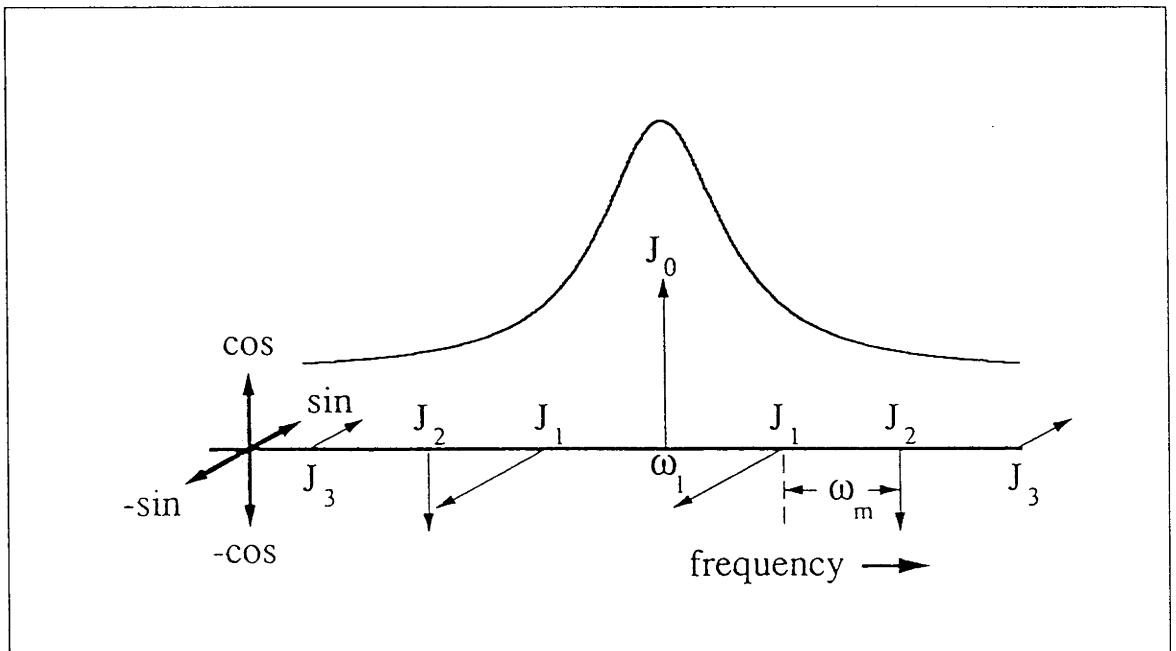


Figure 2.9: Fourier spectrum of phase modulation

The Lorentzian profile of maximum inversion is shown superimposed on the phase modulation Fourier spectrum. The amplitudes of all sidebands and carrier are given by the Bessel function $J_n(A)$. The length of the vectors shows the relative strength of the carrier and sideband components given by these Bessel functions.

$$\begin{aligned}
& + \sum_{n=0}^{\infty} (-1)^{n+1} J_{2n+1}(A) [\sin((\omega_a - (2n+1)\omega_m)t) + \sin((\omega_a + (2n+1)\omega_m)t)] \\
& + \sum_{n=1}^{\infty} (-1)^n J_{2n}(A) [\cos((\omega_a - 2n\omega_m)t) + \cos((\omega_a + 2n\omega_m)t)], \quad (2.32)
\end{aligned}$$

where $J_n(A)$ is the n -th order Bessel function. Eq. (2.32) shows that the phase modulated light is equivalent to resonant light with an amplitude of $J_0(A)E_0$ plus non-resonant light at the sideband frequencies with amplitudes $\pm J_n(A)E_0$ as shown in Fig. 2.9. Similarly the Bloch equations (2.30) can be written as,

$$\begin{aligned}
\dot{u} &= -\Omega_0 \left[2 \sum_{n=0}^{\infty} (-1)^n J_{2n+1}(A) \cos((2n+1)\omega_m t) \right] w, \\
\dot{v} &= \Omega_0 J_0(A) w \\
& \quad + \Omega_0 \left[2 \sum_{n=1}^{\infty} (-1)^n J_{2n}(A) \cos(2n\omega_m t) \right] w, \\
\dot{w} &= -\Omega_0 J_0(A) v \\
& \quad - \Omega_0 \left[2 \sum_{n=1}^{\infty} (-1)^n J_{2n}(A) \cos(2n\omega_m t) \right] v \\
& \quad + \Omega_0 \left[2 \sum_{n=0}^{\infty} (-1)^n J_{2n+1}(A) \cos((2n+1)\omega_m t) \right] u. \quad (2.33)
\end{aligned}$$

Note that in this rotating frame, the even order sidebands couple the atomic inversion with the in-quadrature dipole moment whereas the odd order sidebands couple the atomic inversion with the in-phase dipole moment. An analytic solution of these equations is not known, so we need to solve them numerically.

Unlike the previous case complete inversion can occur for *any* phase modulation frequency. No inequality restricts the occurrence of phase modulation correlated sideband inversion. Fig. 2.10 presents a numerical solution of Eqs. (2.30) showing complete atomic inversion by the correlated sideband mechanism. The phase modulation index is chosen to be the first zero of the zeroth order Bessel function, $J_0(A_0) = 0$, where $A_0 \approx 2.405$. Hence according to the Fourier decomposition Eq. (2.32) no resonant light is present. The phase modulation frequency has been chosen arbitrarily to be equal to the resonant Rabi frequency, $\omega_m = \Omega_0$. Fig. 2.10 shows a small rapid oscillation superimposed on a larger slower oscillation. Numerically, we found that increasing the modulation frequency ω_m increases the rapid oscillation frequency but reduces its amplitude. Increasing the modulation frequency also increases the inversion period, i.e., the time for complete inversion from an initial ground state.

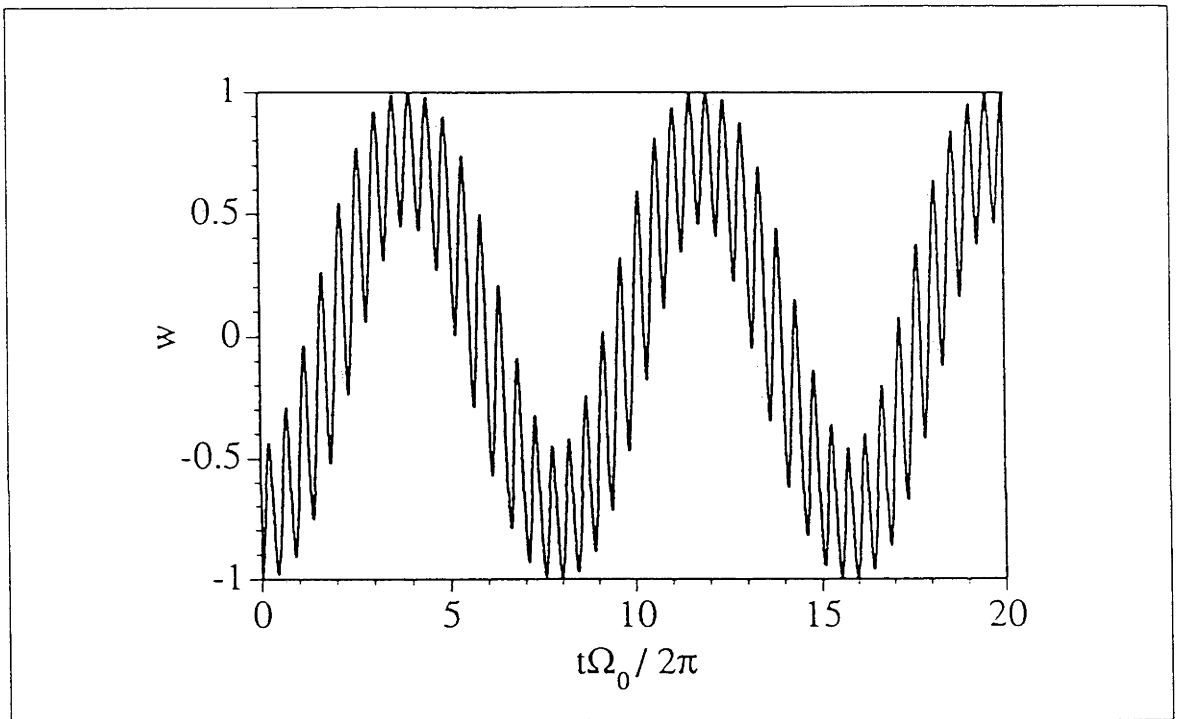


Figure 2.10: Atomic population inversion for phase modulated light

Atomic population inversion w as a function of dimensionless time for a two-level atom driven by phase modulation correlated sideband light, Eq. (2.29), with $\omega_m = \Omega_0$. The light is phase modulated resonant light with modulation index A_0 , $J_0(A_0) = 0$, so that all power is in the sidebands. w is obtained by numerically solving Eqs. (2.30). Complete atomic inversion is achieved for $t\Omega_0/2\pi \approx 4$.

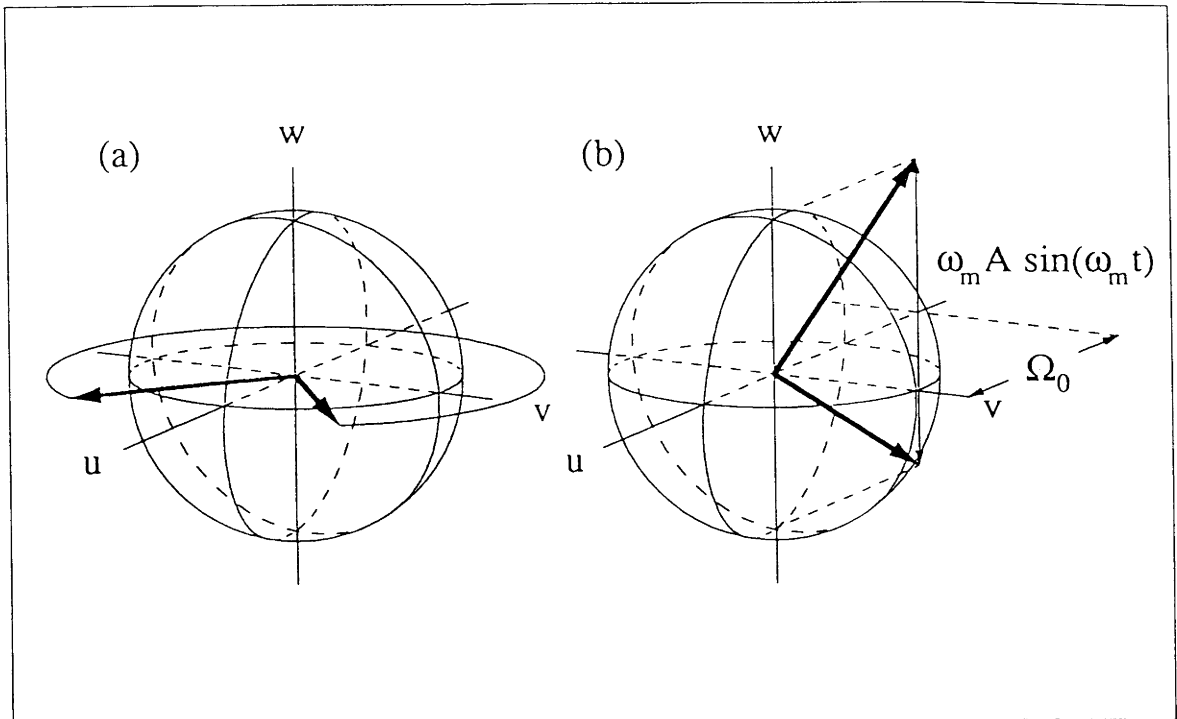


Figure 2.11: The effective torque field for phase modulated driving

(a) The effective torque field of the phase modulated driving oscillates in the uv -plane, $\tau = (-\Omega_0 \cos(A_0 \cos \omega_m t), -\Omega_0 \cos(A_0 \cos \omega_m t), 0)$. When transformed to the phase modulated rotating frame, (b) shows that the effective torque field becomes $\tau = (-\Omega_0, 0, \omega_m A \sin \omega_m t)$.

2.7 Phase modulation: Phase modulated rotating frame

The correlated sideband inversion induced by phase modulated light can be understood using the Bloch sphere picture if we switch to a frequency modulated rotating frame [6]. This is done by replacing the $\omega_l t$ terms in Eq. (2.4) with $\omega_l t + A \cos \omega_m t$. In this frame the effective field is given by,

$$\tau = (-\Omega_0, 0, \omega_m A \sin \omega_m t) \quad (2.34)$$

This is similar to the single detuned sideband case Eq. (2.16), except that the w -component is oscillating about zero at the modulation frequency Fig. 2.11. This is the crucial difference that makes complete inversion possible. The constant u -component alone would cause complete inversion, but the effect of the oscillating w -component does not simply average to zero. It moves the Bloch vector out of the v - w plane, reducing the effective strength of the u -component of τ and hence increasing the inversion period. The inversion period increases with the modulation frequency because the w -component of the effective field is proportional to the modulation frequency, Eq. (2.34).

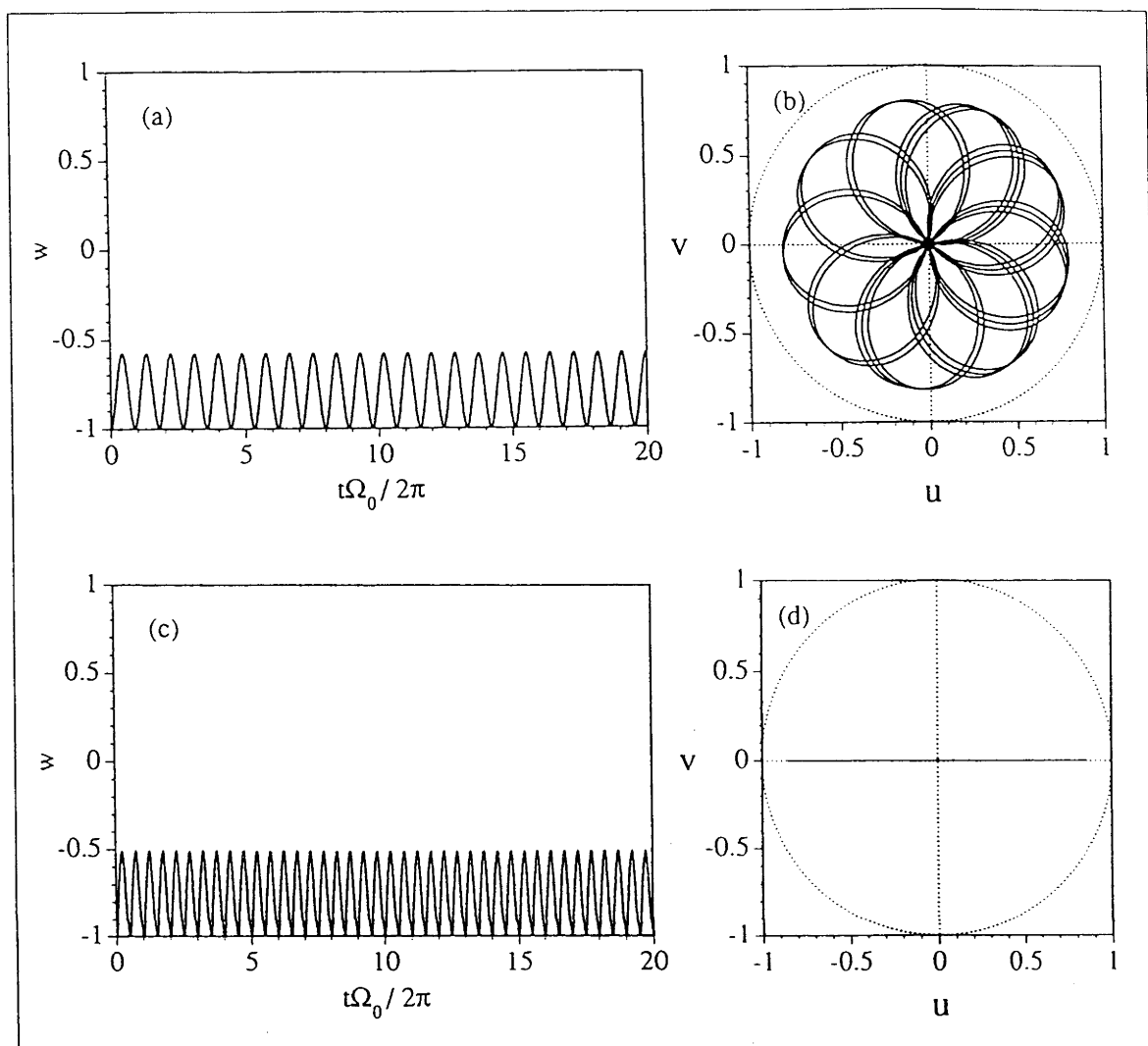


Figure 2.12: Effects of individual sidebands on the two-level atom I
 A two-level atom driven by (a) & (b): S_1 and (c) & (d): $S_1 + S_2$. The modulation frequency $\omega_m = \Omega_0$. Complete atomic inversion is not achieved in both (a) & (c).

The rapid oscillation of the inversion is thus caused by the oscillatory w -component.

2.8 Phase modulation: Sideband analysis

Most of the behaviour of the correlated sideband inversion induced by phase modulated light can be accounted for by the first two pairs of sidebands. Fig. 2.13g shows the atomic population inversion when,

$$\mathcal{E}(t) = S_1 + S_2 + S_3 + S_4, \quad (2.35)$$

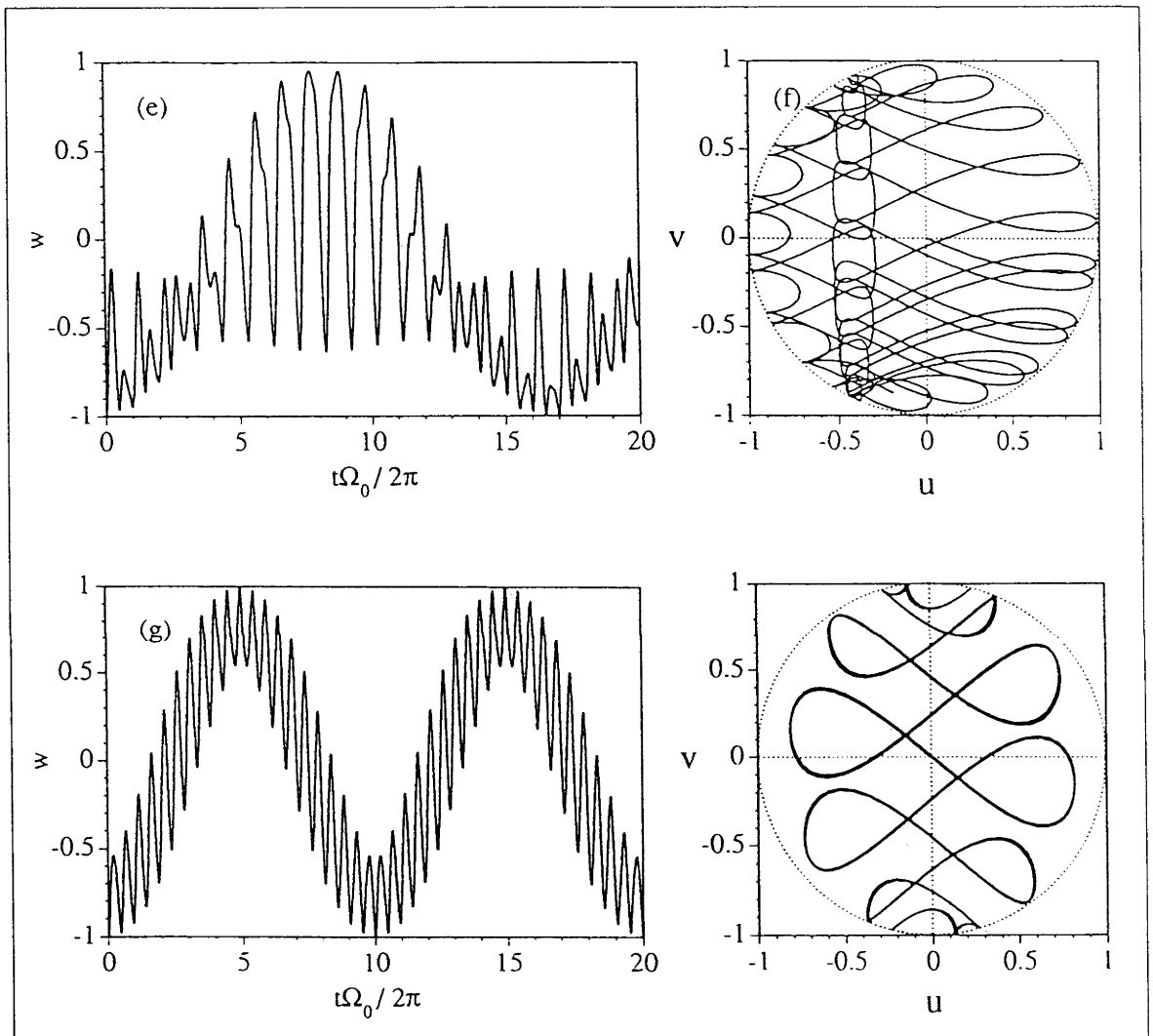


Figure 2.13: Effects of individual sidebands on the two-level atom II
 A two-level atom driven by (e) & (f): $S_1 + S_2 + S_3$ and (g) & (h): $S_1 + S_2 + S_3 + S_4$.
 The modulation frequency $\omega_m = \Omega_0$. Complete atomic inversion is achieved in (g) in only 5
 normal Rabi period.

where,

$$S_1 = -J_1(A_0)[\sin((\omega_a + \omega_m)t)], \quad (2.36)$$

$$S_2 = -J_1(A_0)[\sin((\omega_a - \omega_m)t)], \quad (2.37)$$

$$S_3 = -J_2(A_0)[\cos((\omega_a + 2\omega_m)t)], \quad (2.38)$$

$$S_4 = -J_2(A_0)[\cos((\omega_a - 2\omega_m)t)]. \quad (2.39)$$

Comparison with Fig. 2.10 shows that the behaviour of the inversion in the phase modulated case is approximately reproduced. Our numerical work shows that as long as two pairs of sidebands exist, one of which is odd order and the other even order, correlated sideband inversion is possible for *any* modulation frequency. With the two pairs of sidebands, Eq. (2.35), the effective field, in the uniformly rotating frame Eq. (2.4), is

$$\tau = 2\Omega_0(J_2(A) \cos(2\omega_m t), -J_1(A) \cos(\omega_m t), 0). \quad (2.40)$$

This effective field vector describes a curve in the u - v plane, not a line through the origin as in the case of the single sideband pair Eq. (2.28). This change breaks the symmetry that was previously responsible for periodically undoing the small increments in the atomic inversion, and hence a “secular” increase becomes possible. Since the inversion is coupled to v only by even order sidebands and to u only by odd order sidebands, such secular increase is only possible when the driving field contains both even and odd order sidebands.

2.9 Effect of spontaneous emission

Since we are interested in the experimental feasibility of correlated sideband inversion in the optical regime we now consider the effect of atomic spontaneous emission. Spontaneous emission at rate γ is modeled by respectively adding the three terms $-\gamma u/2$, $-\gamma v/2$, and $-\gamma(w+1)$ to the three right hand sides of Eqs. (2.5, 2.6, 2.7). Fig. 2.14 and Fig. 2.15 shows the effect of spontaneous emission on the inversion for phase modulation correlated sideband driving and for detuned monochromatic driving. Although spontaneous emission of the two-level atom suppresses complete inversion, it does not completely destroy the effect of correlated sideband inversion. This is shown by the fact that the long time average inversion with correlated sideband driving Fig. 2.15 is larger than with monochromatic driving Fig. 2.14. The case of symmetrically detuned sideband pair driving with spontaneous emission is also shown in comparison with monochromatic detuning in Fig. 2.16 and 2.17.

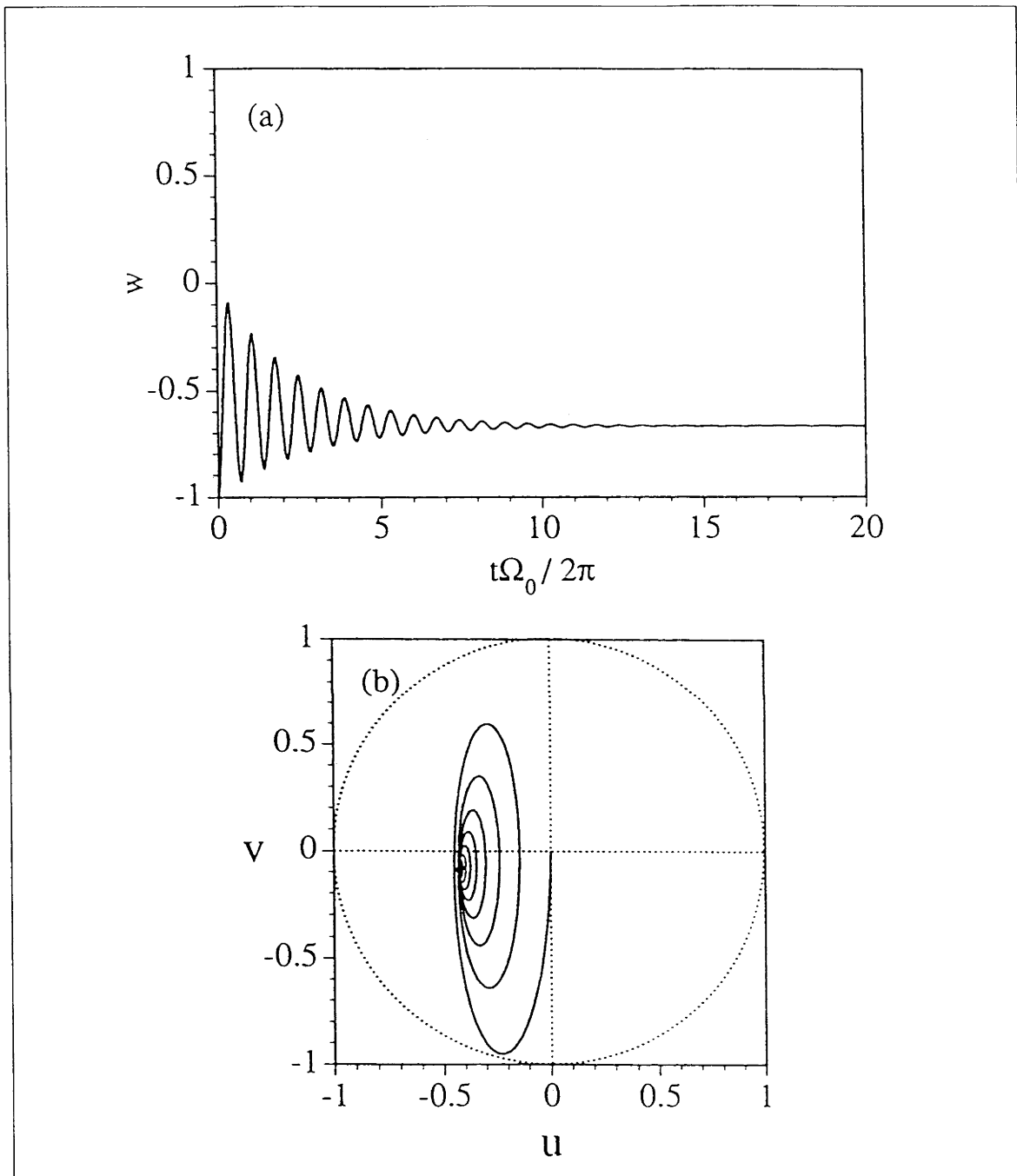


Figure 2.14: Monochromatic driving with spontaneous emission

The spontaneous emission rate $\gamma = 0.1\Omega_0$. (a) atomic population inversion w as a function of dimensionless time and (b) the plot of atomic dipole phase space, for monochromatic detuned driving, $\delta = \Omega_0$. For the asymptotic time averaged $\langle w \rangle \approx -0.67$.

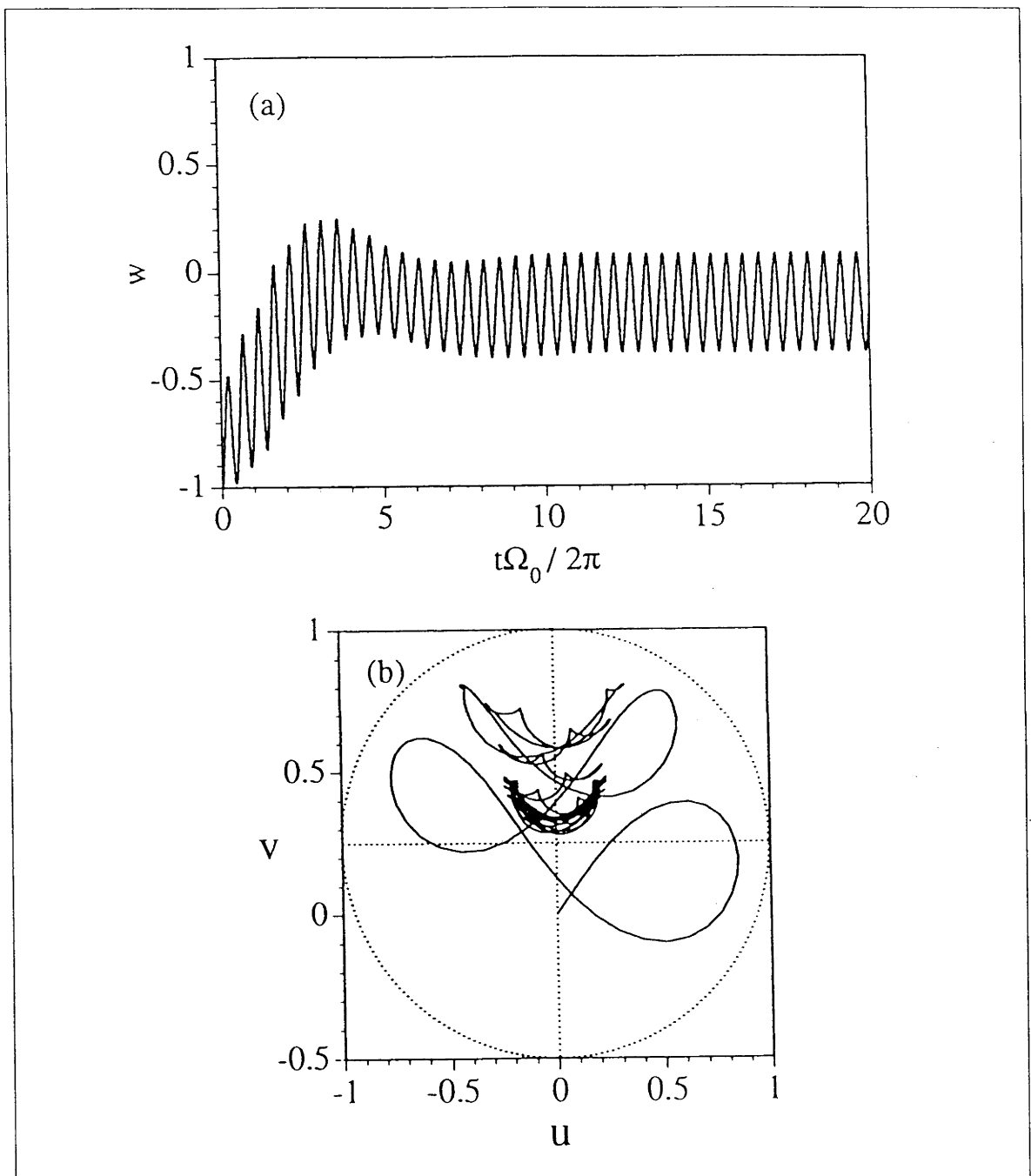


Figure 2.15: Phase modulated driving with spontaneous emission

The effect of spontaneous emission, $\gamma = 0.1\Omega_0$. (a) atomic population inversion w as a function of dimensionless time and (b) the plot of atomic dipole phase space, for phase modulated driving, Eq. (2.29), with modulation index A_0 and $\omega_m = \Omega_0$. For the asymptotic time averaged inversion is $\langle w \rangle \approx -0.15$

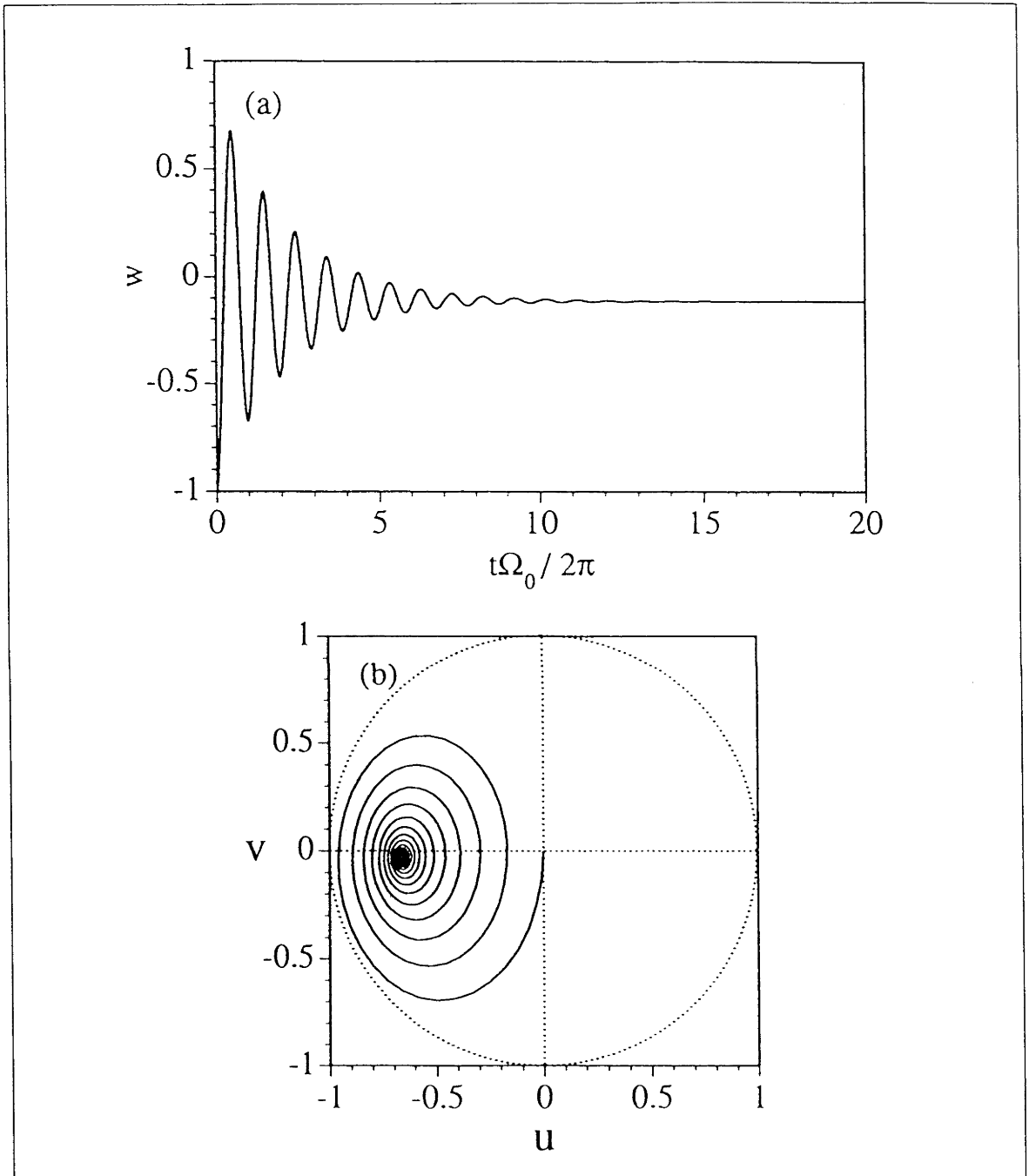


Figure 2.16: Monochromatic driving with spontaneous emission

The spontaneous emission rate $\gamma = 0.1\Omega_0$. (a) atomic population inversion w as a function of dimensionless time and (b) the plot of atomic dipole phase space, for monochromatic detuned driving, $\delta = 0.25\Omega_0$.

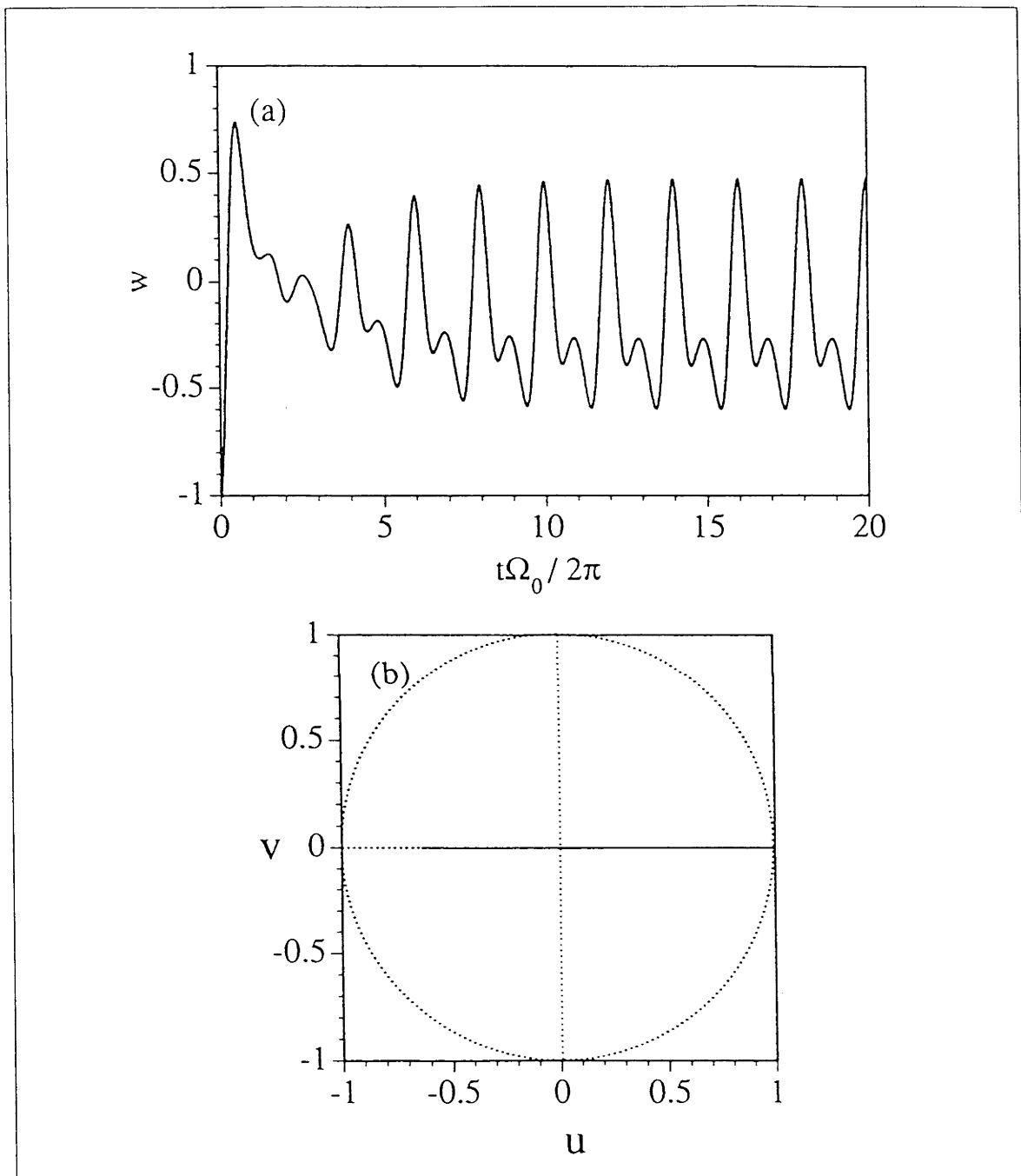


Figure 2.17: Symmetrical sideband driving with spontaneous emission
 The spontaneous emission rate $\gamma = 0.1\Omega_0$. (a) atomic population inversion w as a function of dimensionless time and (b) the plot of atomic dipole phase space, for symmetrically detuned sideband pair with modulation frequency $\omega_m = 0.50\Omega_0$.

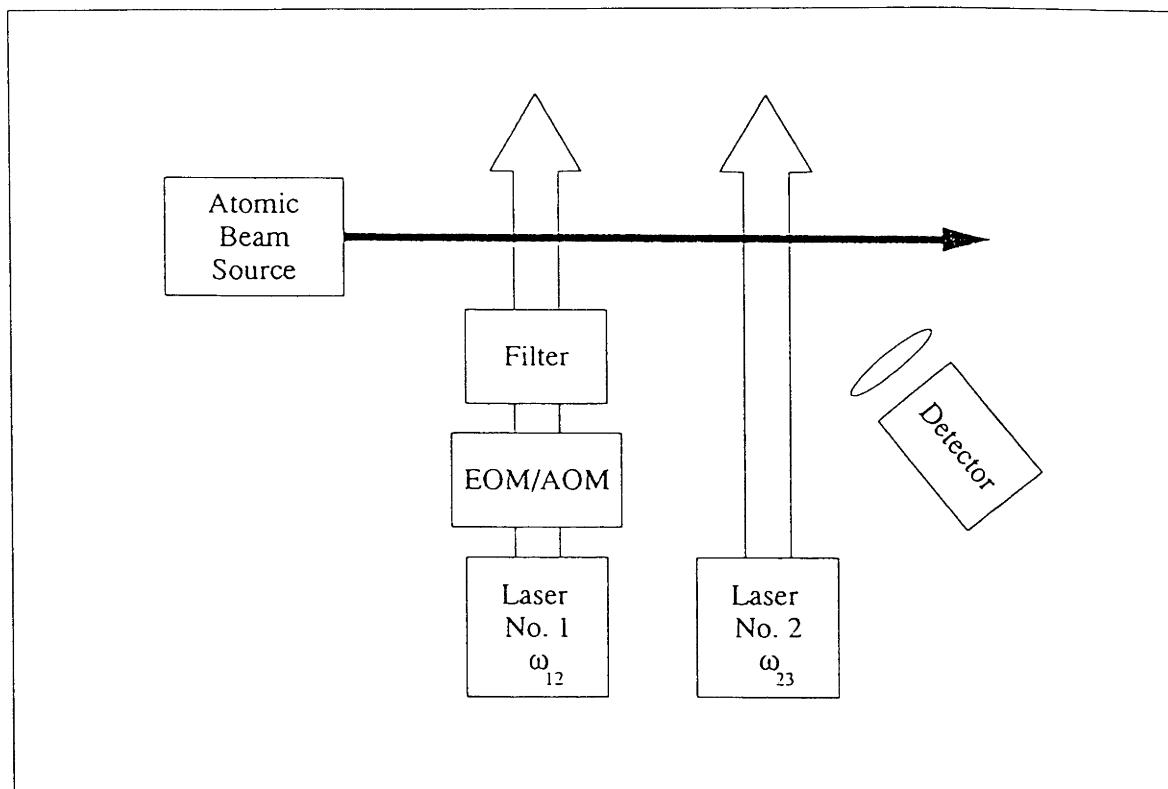


Figure 2.18: Experimental setup for correlated sideband inversion demonstration

2.10 Outline of experiment

We conclude this chapter with an outline of an optical experiment in which correlated sideband inversion could potentially be observed. Fig. 2.18 shows such an experimental setup.

A laser tuned to the atomic resonance can be phase modulated (or amplitude modulated) as required with an electro-optic modulator (acousto-optic modulator). The required modulation amplitude $A_0 \approx 2.4$ is easily achieved with a resonant modulator. An atomic filter could be used to ensure that no resonant component is left. In order to observe correlated sideband inversion the light-atom interaction time must be controlled. This is possible using either a cw laser and a velocity selected (cooled) atomic beam or a pulsed laser and a thermal atomic beam. The inversion could be detected by standard hot wire or laser induced fluorescence techniques, for example.

In summary we have predicted that complete atomic population inversion can be induced in a two-level atom by driving it with correlated non-resonant sidebands. This correlated sideband inversion should be experimentally testable. In the remaining chap-

ters, we will discuss this effect in the context of other two-state quantum and photonic systems.

Chapter 3

Suppression of Quantum Tunneling

3.1 Overview

The phenomenon of quantum tunneling has been known since the early heyday of quantum mechanics. Hund [3] in 1927 explained that the observed splitting of the vibration spectra of ammonia NH_3 was due to quantum tunneling and that quantum tunneling is important for the intramolecular rearrangement of atoms in pyramidal molecules in general.

However, it was only until very recently that the phenomenon of quantum tunneling was found to be controllable by periodic perturbation. More importantly, if the periodic perturbation satisfies certain conditions, quantum tunneling can be completely suppressed. This result was first reported by Grossmann et. al. [24, 25]. Their investigation was on the effect of a monochromatic driving force on the tunneling of a particle in a symmetric double-well potential. The Hamiltonian of their system was given by

$$\hat{\mathcal{H}}(x, p) = \frac{1}{2}p^2 - \frac{1}{4}x^2 + \frac{x^4}{64D} + xS \sin \omega t, \quad (3.1)$$

where S is the amplitude of the perturbation and D is a barrier height parameter. This Hamiltonian is of fundamental interest because it can be used to model proton transfer in atoms and molecules, inversion motion of atoms in pyramidal molecules, as well as other mesoscopic systems (ac-driven SQUIDs).

In both their papers [24, 25], the Floquet formalism and the concept of quasienergy were used. By first defining a propagator for small enough time steps, they were able to

obtain a stroboscopic description of the particle's motion in the double-well. The initial state of the system chosen was to position a particle with a Gaussian centre in one of the wells. It was found that in certain cases even after twenty normal tunneling periods, the particle remained localized in the same well. However, their work was mainly numerical and no physical explanation was offered to explain the newly discovered phenomenon. The condition for the suppression of tunneling was found to be the exact crossing of the two Floquet ground states, Φ_e and Φ_o , and no analytic expressions were given.

Among other results, they also observed that gradual tunneling still occurs even at the exact crossing of the two Floquet ground states. They attributed this gradual tunneling to the fact that their chosen initial state, the Gaussian state, is not exactly the superposition state of the two Floquet eigenstates, $\frac{1}{\sqrt{2}}\Phi_e + \Phi_o$.

In this chapter, we will make use of the two-level approximation of the quantum double-well [28, 27] to relate the phenomenon of the suppression of tunneling to the work of the correlated sideband inversion of a two-level atom. This simplification of the quantum double-well enables us to find an analytic expression for the conditions needed for the suppression of quantum tunneling. Furthermore, we will show that the gradual tunneling of particles even at the tunneling suppression conditions is not solely due to the initial Gaussian state of the wavefunction, but rather it is also due to a phenomenon analogous to the correlated sideband inversion in the two-level atom model. Finally, we also relate the two-level atom model to the work of the low-frequency radiation generation scheme proposed by Dakhnovskii and Metiu [31]. Again because of an analogy to the correlated sideband inversion of the two-level atom, we are able to extend the proposed parameter regime of the low-frequency radiation generation.

3.2 2-level approximation of quantum double-well

A two-level approximation of the double-well potential is given by the Hamiltonian [28, 27]

$$\mathcal{H} = -\frac{\Delta_0}{2} (|1\rangle\langle 1| - |2\rangle\langle 2|) + V(t) (|1\rangle\langle 2| + |2\rangle\langle 1|), \quad (3.2)$$

where $|1\rangle$ and $|2\rangle$ are the two lowest energy eigenstates of the double-well and Δ_0 is the energy splitting between them. The two eigenstates are coupled to each other due to the presence of an external periodic driving force $V(t) = V_0 \sin(\omega t)$. In this model,

the localization of a particle in the “right” and “left” well are represented by the states

$$|r\rangle = \frac{1}{\sqrt{2}}(|1\rangle + |2\rangle), \quad (3.3)$$

$$|l\rangle = \frac{1}{\sqrt{2}}(|1\rangle - |2\rangle), \quad (3.4)$$

respectively. This two-level approximation of the double-well is valid provided that the driving frequency ω and the energy splitting Δ_0 of the two levels is small compare to the energy of the other higher excited levels.

Using the perturbation method, the first order approximation to the period propagator matrix U of the system in the basis set of $\{|r\rangle, |l\rangle\}$ can be shown to take the form of [28]

$$U_{11} = 1, \quad (3.5)$$

$$U_{22} = 1, \quad (3.6)$$

$$U_{12} = \frac{\pi i \Delta_0}{\omega} \exp\left(\frac{-2iV_0}{\omega}\right) J_0\left(\frac{2V_0}{\omega}\right), \quad (3.7)$$

$$U_{21} = -U_{12}^*. \quad (3.8)$$

This is a good approximation provided that the period is small enough to not have caused significant changes in the state amplitudes. Hence, quantum tunneling is suppressed when

$$\frac{2V_0}{\omega} = j_{0,m} \quad (3.9)$$

and

$$\Delta_0 \ll 2\omega \quad (3.10)$$

where $j_{0,m}$ is the m -th root of the zeroth order Bessel function.

3.3 Analogy with the two-level atom

We now relate our work on the two-level atom to the suppression of quantum tunneling. Our two-level atom Hamiltonian Eq. (2.1) gives the following equations of motion for the amplitudes c_g to be in the ground state and c_e to be in the excited state,

$$i \dot{c}_e = \frac{1}{2}\omega_a c_e - \frac{1}{\hbar}dE(t)c_g, \quad (3.11)$$

$$i \dot{c}_g = -\frac{1}{\hbar}dE(t)c_e - \frac{1}{2}\omega_a c_g. \quad (3.12)$$

Using dashes to denote rotating variables defined by,

$$c'_e = \exp\left[\frac{1}{2}i(\omega_a t + A \cos \omega_m t)\right]c_e, \quad (3.13)$$

$$c'_g = \exp\left[-\frac{1}{2}i(\omega_a t + A \cos \omega_m t)\right]c_g, \quad (3.14)$$

we obtain for the phase modulated field $E(t) = E_0 \cos(\omega_a t + A \cos \omega_m t)$,

$$i \dot{c}'_e = \frac{1}{2}A\omega_m \sin(\omega_m t)c'_e - \frac{1}{2}\Omega_0 c'_g, \quad (3.15)$$

$$i \dot{c}'_g = -\frac{1}{2}\Omega_0 c'_e - \frac{1}{2}A\omega_m \sin(\omega_m t)c'_g, \quad (3.16)$$

where we have used the rotating wave approximation to neglect rapidly rotating terms proportional to $\exp(2i(\omega_a t + A \cos \omega_m t))$.

The equations of motion for quantum tunneling in a modulated double-well, in the two-level approximation, are

$$i \dot{c}_r = V_0 \sin(\omega t)c_r - \frac{1}{2}\Delta_0 c_l, \quad (3.17)$$

$$i \dot{c}_l = -\frac{1}{2}\Delta_0 c_r - V_0 \sin(\omega t)c_l, \quad (3.18)$$

where c_r and c_l are the amplitudes of the right and left well states $|r\rangle$ and $|l\rangle$, respectively. A comparison of Eqs. (3.15, 3.16) and Eqs. (3.17, 3.18) shows the mathematical equivalence of the two models by making the following state correspondence,

$$c'_e \leftrightarrow c_r, \quad (3.19)$$

$$c'_g \leftrightarrow c_l. \quad (3.20)$$

The correspondence between parameters is,

$$\omega_m \leftrightarrow \omega, \quad (3.21)$$

$$\Omega_0 \leftrightarrow \Delta_0, \quad (3.22)$$

$$A \leftrightarrow 2V_0/\omega. \quad (3.23)$$

The conditions for good localization in a single well Eqs. (3.9, 3.10) simply correspond in our model to a zero amplitude carrier component and a large modulation frequency. The suppression of quantum tunneling in a double-well potential is therefore analogous in our atomic system to modulating away the resonant component of the radiation field and hence suppressing any excitation of the atom. Because of the equivalent effect to correlated sideband inversion, the localization of a particle in one well will always be limited in duration, a result not apparent in the perturbative treatment of [28].

3.4 Low-frequency radiation generation

Dakhnovskii and Metiu [31] has proposed that by driving a charged particle in a double well with laser, intense low-frequency radiation can be produced . Again the two-level approximated Hamiltonian is used,

$$\mathcal{H} = \varepsilon (|1\rangle\langle 1| - |2\rangle\langle 2|) - \mu_{12}E(t) (|1\rangle\langle 2| + |2\rangle\langle 1|), \quad (3.24)$$

where μ_{12} is the induced dipole moment, $E(t)$ is electric field and 2ε the energy splitting.

Similarly there is a correspondence between the two-level atom model and this,

$$\omega_m \leftrightarrow \omega, \quad (3.25)$$

$$\Omega_0 \leftrightarrow 2\varepsilon/\hbar, \quad (3.26)$$

$$A \leftrightarrow e_0, \quad (3.27)$$

where ω is the driving laser frequency, and $e_0 = 2\mu_{12}E_0/\hbar\omega$ is proportional to the laser amplitude. Accordingly their conditions for low frequency generation, $\varepsilon/\hbar\omega \ll 1$ and $\varepsilon J_0(e_0)/\hbar$ small, correspond in our model to having highly detuned sidebands and a small component of resonant carrier, which induces a low frequency Rabi oscillation. The analogous effect to our correlated sideband inversion occurs in their model for $\varepsilon J_0(e_0)/\hbar = 0$. Furthermore it occurs for arbitrary values of $\varepsilon/\hbar\omega$. This extends the parameter regime for low frequency generation to the point of accidental degeneracy [31] and to arbitrary driving laser frequencies.

Chapter 4

Bloch representation of optical couplers

4.1 Overview

“ Men’s labour therefore should be turned to the investigation and observation of the resemblances and analogies of things. . . for these it is which detect the unity of nature, and lay the foundation for the constitution of the sciences.” Francis Bacon.

The analogy between mechanics and wave theory is long established and has been used to transport knowledge between the two fields. More than a century ago, James Clark Maxwell draws upon a mechanical analogy when developing his electromagnetic theory [1]. In the early days of quantum mechanics, many made use of concepts from wave optics to explain the newly formulated quantum theory. More recently, the analogy between quantum mechanics and optics has yet again been studied in a new framework of optical waveguide theory. Black and Ankiewicz [11] show that in the respective length and time independent case, the scalar wave equation and the Schrödinger equation are mathematically equivalent. One-to-one correspondence is found between the quantities of the two models.

In this chapter, we re-establish the one-to-one correspondence between the quantities in quantum mechanics and wave optics. Our starting point is also a comparison of the two most important equations of the respective fields, namely, the Schrödinger equation and the scalar wave equation. However, we do not wish to limit ourselves to the length/time independent case. With the help of the slow varying envelope

approximation, we proceed to establish a correspondence of the quantities between the two models when they are length/time dependent. This chapter hence plays the important role of a bridge linking the two parts of this thesis.

We continue with the comparison of a four-port optical coupler and a potential double-well. It is found that the four-port optical coupler has many similar characteristics to the potential double-well in quantum mechanics. Quantum tunneling, for example, is translated to the well understood phenomenon of power transfer between the two cores of an optical coupler. Finally, we translate the Bloch representation used for analysing the two-level atom to a new representation for the optical state in a coupler. This Bloch representation of the optical coupler is a convenient tool for visualizing the evolution of the optical state. As an example of the application of this new representation, we consider the case of a uniform coupler. In the next chapter, we also use this representation to consider a coupler with two out-of-phase sinusoidally modulated core indices.

4.2 The Schrödinger equation and the scalar wave equation

In this section, we establish the mathematical correspondence between the Schrödinger equation,

$$-\frac{\hbar^2}{2m}\nabla^2\Psi + V\Psi = i\hbar\frac{\partial}{\partial t}\Psi, \quad (4.1)$$

and the scalar wave equation,

$$\nabla^2\Psi + k^2n^2\Psi = 0. \quad (4.2)$$

The quantity Ψ in the Schrödinger equation is the wavefunction of a particle. Whereas in the scalar wave equation, Ψ represents the complex wave amplitude of the electric field. m is the mass of the particle and \hbar the Planck constant. In the scalar wave equation k denotes the wavenumber and n is the refractive index of the medium. We are interested to establish a one-to-one correspondence between the two equations so that in the later chapters, concepts from the work on quantum tunneling and correlated sideband inversion can be applied to the wave optics model of optical couplers. We start our comparison with the case when both of these equations are time independent. We thus require the potential of the Schrödinger equation to be time independent and

the refractive index of the wave equation to be constant along the entire propagation length z . The two equations in the time/length independent case are

$$\nabla^2\Psi + \frac{2m}{\hbar^2}(E - V)\Psi = 0, \quad (4.3)$$

and

$$\nabla_i^2\Psi + (k^2n^2 - \beta^2)\Psi = 0. \quad (4.4)$$

Here E is the total energy of the particle and β is the propagation constant of the electric field. Note that in simplifying the scalar wave equation to the length independent case, we have removed the z -dependence of the scalar wave equation and hence are left with

$$\nabla_i^2 = \frac{\partial^2}{\partial x^2} + \frac{\partial^2}{\partial y^2} \quad (4.5)$$

on the left hand side of Eq. (4.4). If we assume that the Schrödinger equation is two dimensional, the correspondence is easily found to be,

$$-\frac{2m}{\hbar^2}V \leftrightarrow k^2n^2 \quad (4.6)$$

$$-\frac{2m}{\hbar^2}E \leftrightarrow \beta^2 \quad (4.7)$$

$$x \leftrightarrow x \quad (4.8)$$

$$y \leftrightarrow y \quad (4.9)$$

We observe that the square of the refractive index in wave optics is analogous to an inverted potential energy and the total energy in quantum mechanics is analogous to the inverted squared propagation constant. If the above correspondence were made, problems and solutions in quantum mechanics will have a corresponding counterpart in wave optics.

However, we observe that when the Schrödinger equation and the scalar wave equation become time/length-dependent, the correspondence is no longer obvious due to the difference in the first order and the second order derivative terms on the right hand side of Eqs (4.1, 4.2). This apparent discrepancy can be resolved if we assume that the complex electric field amplitude in the scalar wave equation has the following form,

$$\Psi(z) = \psi(z)e^{i\int\beta dz}, \quad (4.10)$$

so that

$$\frac{\partial}{\partial z}\Psi(z) = \left[\frac{\partial}{\partial z}\psi(z) + i\beta\psi(z) \right] e^{i\int\beta dz}, \quad (4.11)$$

and

$$\frac{\partial^2}{\partial z^2}\Psi(z) = \left[\frac{\partial^2}{\partial z^2}\psi(z) + 2i\beta\frac{\partial}{\partial z}\psi(z) + i\psi(z)\frac{\partial}{\partial z}\beta - \beta^2\psi(z) \right] e^{i\int\beta dz}. \quad (4.12)$$

The scalar wave equation is now of the form

$$\nabla_t^2 \psi(z) + (k^2 n^2(z) - \beta^2(z)) \psi(z) = - \left[\frac{\partial^2}{\partial z^2} \psi(z) + 2i\beta(z) \frac{\partial}{\partial z} \psi(z) + i\psi(z) \frac{\partial}{\partial z} \beta(z) \right]. \quad (4.13)$$

If we assume that the envelope function $\psi(z)$ is varying sufficiently slowly for the slowly-varying envelope approximation (SVEA) to be valid, we can then neglect the second order partial derivative $\partial^2 \psi / \partial z^2$. Furthermore the term $i\psi(z) \partial \beta(z) / \partial z$, which is responsible for the coupling of the forward-propagating modes to the backward-propagating modes, can also be ignored by assuming that the change in the refractive index profile along the direction of propagation is slow compared to the evolution of the envelope function. The scalar wave equation is therefore reduced to

$$\nabla_t^2 \psi(z) + (k^2 n^2(z) - \beta^2(z)) \psi(z) = -2i\beta(z) \frac{\partial}{\partial z} \psi(z). \quad (4.14)$$

By also assuming that the wavefunction of a particle in quantum mechanics can be written as,

$$\Psi(t) = \psi(t) e^{i \int E(t) dt / \hbar}, \quad (4.15)$$

The Schrödinger equation can then be rewritten as,

$$\nabla^2 \psi(t) + \left(-\frac{2m}{\hbar^2} V(t) + \frac{2m}{\hbar^2} E(t) \right) \psi(t) = i \frac{2m}{\hbar} \frac{\partial}{\partial t} \psi(t). \quad (4.16)$$

Once again, we can obtain a correspondence of all the quantities between the two equations,

$$-2mV(t) \leftrightarrow n^2, \quad (4.17)$$

$$-2mE(t) \leftrightarrow \lambda^2 \beta^2, \quad (4.18)$$

$$-\frac{\partial}{\partial t} \leftrightarrow \frac{\partial}{\partial z}, \quad (4.19)$$

$$\Psi(t) \leftrightarrow \Psi(z), \quad (4.20)$$

$$\psi(t) \leftrightarrow \psi(z), \quad (4.21)$$

$$mt \leftrightarrow \lambda \beta z, \quad (4.22)$$

$$x \leftrightarrow x, \quad (4.23)$$

$$y \leftrightarrow y, \quad (4.24)$$

$$\hbar \leftrightarrow \lambda, \quad (4.25)$$

where $\lambda = \lambda / 2\pi$. It is interesting to note in particular, that the Planck constant which plays a crucial role in quantum mechanics has also an analogous quantity in wave

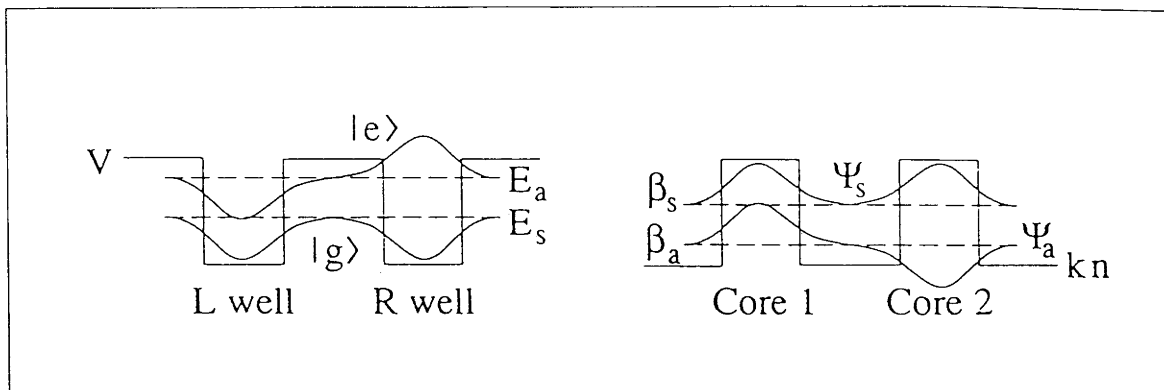


Figure 4.1: The double wells of quantum mechanics and wave optics

optics which is entirely classical. We see that when the wavelength of the electric field is short (corresponding to $\hbar \rightarrow 0$), the “quantum features” of wave optics disappear and the wave optics is then replaced by the more classical ray optics in this regime. The Planck constant on the other hand is a universal constant and cannot be varied. Hence the quantum properties of a microscopic object are always present. Because of this correspondence between all the quantities of the Schrödinger equation and the scalar wave equation, we can now anticipate interesting results in wave optics analogous to the coherent destruction of quantum tunneling and correlated sideband inversion.

Since the potential energy in quantum mechanics is found to be analogous to the refractive index in wave optics, we anticipate that a quantum double well will in many ways be similar to an optical coupler with the inverted profile, as shown in Fig. 4.1. In particular, if the two-level and two-mode approximation were made on the respective models, we can attribute the power transfer between cores of an optical coupler to a phenomenon similar to quantum tunneling between potential wells. The tunneling period is then found to be analogous to the coupling length of an optical coupler. We give a further listing of the correspondence of other quantities in this case.

$$\text{QUANTUM MECHANICS} \leftrightarrow \text{WAVE OPTICS} \quad (4.26)$$

$$\text{unbound states} \leftrightarrow \text{radiation modes}, \quad (4.27)$$

$$\text{bound states} \leftrightarrow \text{bound modes}, \quad (4.28)$$

$$|g\rangle = \frac{1}{\sqrt{2}}(|r\rangle + |l\rangle) \leftrightarrow \Psi_s = \frac{1}{\sqrt{2}}(\Psi_1 + \Psi_2), \quad (4.29)$$

$$|e\rangle = \frac{1}{\sqrt{2}}(|r\rangle - |l\rangle) \leftrightarrow \Psi_a = \frac{1}{\sqrt{2}}(\Psi_1 - \Psi_2), \quad (4.30)$$

$$|r\rangle = \frac{1}{\sqrt{2}}(|g\rangle + |e\rangle) \leftrightarrow \Psi_1 = \frac{1}{\sqrt{2}}(\Psi_s + \Psi_a), \quad (4.31)$$

$$|l\rangle = \frac{1}{\sqrt{2}}(|g\rangle - |e\rangle) \leftrightarrow \Psi_2 = \frac{1}{\sqrt{2}}(\Psi_s - \Psi_a). \quad (4.32)$$

$$(4.33)$$

4.3 Bloch representation for optical couplers

The evolution of a coherent optical state along a general weakly-guiding, weakly coupled four-port coupler is well modeled by the first order coupled mode theory. Here for generality we consider a coupler with the following coupled mode equations for the field amplitudes in each core

$$\frac{d}{dz}b_1 = i\beta_1(z)b_1 + iC_{12}(z)b_2, \quad (4.34)$$

$$\frac{d}{dz}b_2 = i\beta_2(z)b_2 + iC_{21}(z)b_1, \quad (4.35)$$

where $b_j(z)$ are the complex modal amplitudes and $\beta_j(z)$ are the propagation constants of the fundamental mode of each waveguide taken in isolation from the other, so that the field in each core is described by ($j = 1, 2$)

$$E_j(x, y, z) = b_j(z)\Psi_j(x, y). \quad (4.36)$$

Ψ_j are the fundamental-mode of core j , solutions obtained from the scalar wave equation (4.2). The coupling constants C_{12} and C_{21} in Eq. (4.34, 4.35) are approximately equal in a weakly coupled system, so we may approximate these by $C(z)$. Because $\beta_j(z)$ are comparable to the optical wavenumber, these equations allow us to solve for the rapid absolute phase variation in each core of the coupler. Since we are mainly interested in the much slower power variation induced by the weak power transfer between the cores, and also in the correspondingly slow variation in the relative phase between the fields in each core, we restrict our attention to these “envelopes” by factoring out the rapid optical frequency dependence and transform to the following coupled mode equations

$$\frac{d}{dz}a_1 = i\delta\beta_1(z)a_1 + iC(z)a_2, \quad (4.37)$$

$$\frac{d}{dz}a_2 = i\delta\beta_2(z)a_2 + iC(z)a_1, \quad (4.38)$$

where $a_j(z)$ are the complex amplitudes of the phasors obtained after factoring out the rapid phase variations from $b_j(z)$,

$$a_1(z) = b_1(z)e^{-\beta_1(0)z}, \quad (4.39)$$

$$a_2(z) = b_2(z)e^{-\beta_2(0)z}. \quad (4.40)$$

Also $\delta\beta_j(z) = \beta_j(z) - \beta_j(0)$, where $\beta_j(0)$ denoting the unperturbed or average propagation constant of the fundamental mode for the waveguide j in isolation.

With these equations, we can describe the entire envelope field in the two core system at each position z along the axis, provided we specify the magnitudes of the complex phasors, $|a_1(z)|$ and $|a_2(z)|$, and the relative phase between them $\phi_{12}(z)$. The field amplitudes alone are sufficient to completely specify the power in each core, and for coherent systems, the relative phase $\phi_{12}(z)$ is the only other quantity needed to predict the subsequent evolution of the fields along this coupler. Because these three quantities are needed, this system lends itself to a three-dimensional geometric representation for describing field evolution.

We now introduce a new formalism of using geometric phase to represent the optical field along any optical coupler. We will first show the method of transforming from the coupled mode equations (4.37, 4.38) to the geometric phase representation. Provided that energy is conserved along the length of the coupler, the optical fields trace out a three dimensional sphere similar to that of the Bloch sphere in quantum mechanics and Poincaré sphere in polarization coupling. Hence, we also refer to this representation as the Bloch representation for optical couplers.

We let the local modes of the two cores of the optical coupler be denoted by Ψ_1 and Ψ_2 , respectively. We denote the symmetric and anti-symmetric normal mode of the coupler by Ψ_s and Ψ_a . When light is launched into one core of a coupler with uniform and identical cores so that the initial optical field mode is given by Ψ_1 , we find that at propagation distances of a quarter and three quarters of a coupling period later power is equally shared between the two cores. The optical field modes at these points are given by

$$\Psi_\alpha = \frac{1}{\sqrt{2}}(\Psi_1 + i\Psi_2), \quad (4.41)$$

$$\Psi_\beta = -\frac{1}{\sqrt{2}}(\Psi_1 - i\Psi_2), \quad (4.42)$$

for propagation distances of one quarter and three quarter periods later, respectively. We call these two modes the quadrature modes.

With these three pairs of optical modes, we define an axis for each pair and thus obtained a three-dimensional space with the following axes

$$N = P_s - P_a, \quad (4.43)$$

$$Q = P_\alpha - P_\beta, \quad (4.44)$$

$$P = P_2 - P_1, \quad (4.45)$$

where P_j is simply the power in the j mode given by

$$P_j = a_j^* a_j. \quad (4.46)$$

We use the symbols N, P and Q to help identify the fact that the *power* difference of the two cores is given by the P -axis; the difference between the *normal* modes gives the N value and Q represents the *quadrature* modes difference. Hence for example, N is therefore a measure of the mode symmetry, with $N = P_{\text{total}}$ denoting that all the optical power is in the symmetric mode and $N = -P_{\text{total}}$, the anti-symmetric mode. We can proceed by normalizing the three quantities to unity by dividing each parameter by the total power P_{total} . Hence N, Q and P can only take the values between 1 and -1. A table is given below to show the relationships between these three pairs of modes.

	Ψ_s and Ψ_a	Ψ_α and Ψ_β	Ψ_1 and Ψ_2
$N = 1$	Ψ_s	$\frac{1}{2}[(1-i)\Psi_\alpha - (1+i)\Psi_\beta]$	$\frac{1}{\sqrt{2}}(\Psi_1 + \Psi_2)$
$N = -1$	Ψ_a	$\frac{1}{2}[(1+i)\Psi_\alpha - (1-i)\Psi_\beta]$	$\frac{1}{\sqrt{2}}(\Psi_1 - \Psi_2)$
$Q = 1$	$\frac{1}{2}[(1+i)\Psi_s + (1-i)\Psi_a]$	Ψ_α	$\frac{1}{\sqrt{2}}(\Psi_1 + i\Psi_2)$
$Q = -1$	$-\frac{1}{2}[(1-i)\Psi_s + (1+i)\Psi_a]$	Ψ_β	$-\frac{1}{\sqrt{2}}(\Psi_1 - i\Psi_2)$
$P = 1$	$\frac{1}{\sqrt{2}}(\Psi_s - \Psi_a)$	$-\frac{1}{\sqrt{2}}i(\Psi_\alpha + i\Psi_\beta)$	Ψ_2
$P = -1$	$\frac{1}{\sqrt{2}}(\Psi_s + \Psi_a)$	$\frac{1}{\sqrt{2}}(\Psi_\alpha - \Psi_\beta)$	Ψ_1

In terms of only the local field amplitude, we can express these parameters as

$$N = \frac{a_1 a_2^* + a_1^* a_2}{P_{\text{total}}} \quad (4.47)$$

$$Q = \frac{i(a_1 a_2^* - a_1^* a_2)}{P_{\text{total}}} \quad (4.48)$$

$$P = \frac{a_2^* a_2 - a_1^* a_1}{P_{\text{total}}} \quad (4.49)$$

Assuming that propagation in the coupler is lossless, we obtain

$$N^2 + Q^2 + P^2 = \frac{(a_1^* a_1 + a_2^* a_2)^2}{P_{\text{total}}^2} \quad (4.50)$$

Hence the locus of the optical field of the coupler is a unit sphere. We call the vector (N, Q, P) the optical field vector. The evolution of this field vector is determined entirely by a torque vector which is solely defined by the parameters of the coupler. By substituting the definition of the N, P and Q , Eqs. (4.47, 4.48, 4.49), into the coupled mode equations (4.37, 4.38), we obtain

$$\frac{d}{dz} N = \delta\beta(z) Q, \quad (4.51)$$

$$\frac{d}{dz} Q = -\delta\beta(z) N - 2C(z)P, \quad (4.52)$$

$$\frac{d}{dz} P = 2C(z)Q, \quad (4.53)$$

where $\delta\beta(z) = \delta\beta_1(z) - \delta\beta_2(z)$. It is then straightforward to obtain a torque equation similar to the Larmor equation for magnetic dipole,

$$\vec{O} = \vec{\mathcal{F}} \times \vec{O}. \quad (4.54)$$

where \vec{O} is the optical field vector and $\vec{\mathcal{F}}$ its torque as shown in Fig. 4.2.

4.4 Uniform coupler

We now analyse the case of a uniform non-identical coupler describe by the coupled mode equations

$$\frac{d}{dz} a_1 = i\delta\beta a_1 + iC(z)a_2, \quad (4.55)$$

$$\frac{d}{dz} a_2 = -i\delta\beta a_2 + iC(z)a_1. \quad (4.56)$$

The normal modes of this coupler are given by

$$\Psi_+ = \frac{\Psi_1 + a_+ \Psi_2}{\sqrt{1 + a_+^2}}, \quad (4.57)$$

$$\Psi_- = \frac{\Psi_1 + a_- \Psi_2}{\sqrt{1 + a_-^2}}. \quad (4.58)$$

Here, $a_{\pm} = Q \pm 1/F$, where $Q = \delta\beta/2C$ and $F = (1 + Q^2)^{-1/2}$. By writing down the equivalent torque equation for the system, we find

$$\vec{\mathcal{F}} = (2C, 0, \delta\beta) \quad (4.59)$$

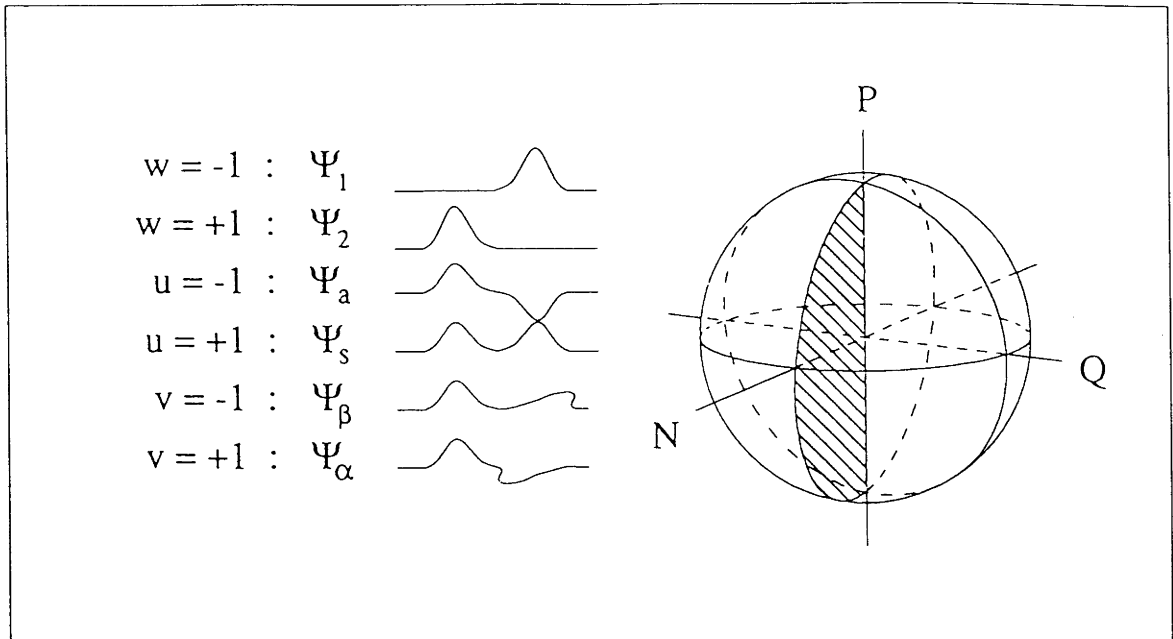


Figure 4.2: The Bloch representation of an optical coupler

Three dimensional sketches of the optical field envelope are shown for the corresponding modes Ψ_j . Note that in the usual rotating frame, the torque vector \vec{F} must have direction lying within the shaded meridian. Since the coupling constant must take a positive value and the propagation constant difference can be either positive or negative.

Note that Ψ_+ and Ψ_- are exactly the point of intersection of the torque vector with the unit sphere of the optical field as shown in Fig. 4.3. This is expected since the only points on the sphere which are unaffected by the torque vectors are the intersection points of the torque with the unit sphere. This simple example illustrates that the Bloch representation provides a clear visualisation of the evolution of the optical field. Using the Bloch representation many quantities of interest can be obtained by solving simple geometric problems without the need to actually integrate the coupled mode equations.

We conclude this chapter by listing the correspondence between the Bloch representation of both the two-level atom and the optical coupler.

$$\text{TWO - LEVEL ATOM} \leftrightarrow \text{OPTICAL COUPLER} \quad (4.60)$$

$$t \leftrightarrow z, \quad (4.61)$$

$$w \leftrightarrow P, \quad (4.62)$$

$$u \leftrightarrow -N, \quad (4.63)$$

$$v \leftrightarrow Q, \quad (4.64)$$

$$\Omega_0 \leftrightarrow 2C, \quad (4.65)$$

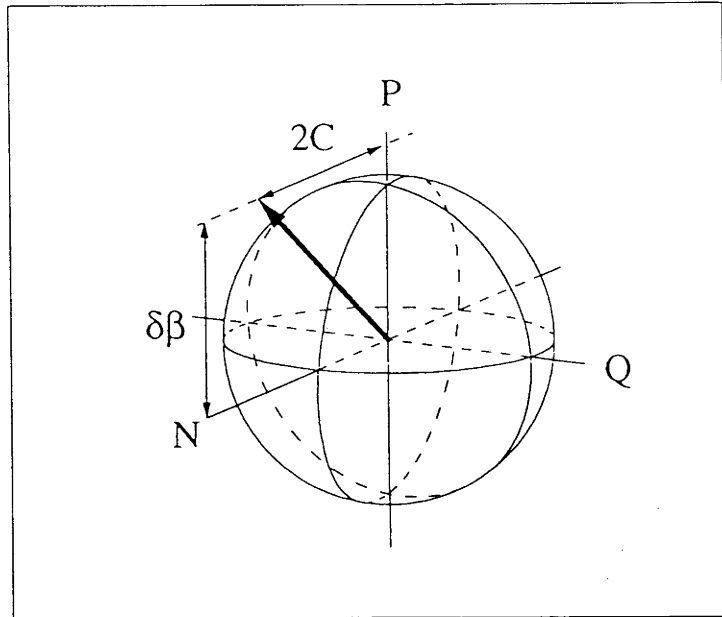


Figure 4.3: The Bloch representation of a uniform non-identical coupler

$$\delta \leftrightarrow \delta\beta, \quad (4.66)$$

$$|g\rangle \leftrightarrow \Psi_1, \quad (4.67)$$

$$|e\rangle \leftrightarrow \Psi_2, \quad (4.68)$$

$$|l\rangle \leftrightarrow \Psi_s, \quad (4.69)$$

$$|r\rangle \leftrightarrow \Psi_a, \quad (4.70)$$

$$\rho \leftrightarrow \vec{O}, \quad (4.71)$$

$$\tau \leftrightarrow \vec{F}. \quad (4.72)$$

With this correspondence, we thus established a link between all three models studied in this thesis.

Chapter 5

Modulated Index Coupler

5.1 Overview

The coupling of light between identical fibres or waveguides is used in a variety of light-combining or splitting devices, such as 3dB couplers, wavelength division multiplexers, broadband and wavelength-flattened couplers and so on. The so-called “grating-assisted coupler” makes use of in-line gratings to cause a periodic modulation of the coupling constant between two dissimilar waveguides to enhance power transfer.

More recently, Bragg gratings have also been employed in conjunction with couplers to suppress or frustrate coupling and form the basis of a new type of channel-dropping filter. The mechanism of the Bragg grating coupler are based solely on the Bragg reflection property of in-line gratings; otherwise propagation along the cores does not take account of the grating. In other words, the grating is assumed to be a sufficiently small perturbation of the refractive-index profile of the guide or coupler so that its effect can be ignored for the purposes of calculating modal fields and propagation parameters. The effect of the grating is that it introduces a strong dispersion in one core and hence causes a phase mismatch between the two cores. At the same time, the Bragg gratings have also created a “photonic” band gap which rejects tunneling photons into the second core.

In this chapter, we present an alternative mechanism for the suppression of coupling, using periodic modulation of core refractive-indices. This new mechanism, in contrast with the Bragg gratings, relies on a relatively large and slow index modulation with

period of the order of $50\mu\text{m}$ – 1mm . Hence, it is necessary to solve for propagation along the cores *taking into account* the variation in the refractive-index profile of the cores. The resultant effect, which can partially or totally frustrate coupling is analogous to the coherent destruction of quantum tunneling discussed in the earlier chapters. Similar to the result found in the suppression of quantum tunneling, we find that the zeroth order Bessel function plays an important role in determining the ratios of the modulation period and amplitude for coupling suppression. Physically, we can view the effect of the index modulation as a mechanism which regulates the modal phase accumulation along the coupler. By judicious choice of the period and amplitude, the index modulation can be so chosen as to completely offset the accumulated phase and thereby suppressed the transfer of power everywhere along the length of the coupler. We will also show that this index modulation is, in a sense, the opposite of the mechanism used in the grating assisted coupler since both mechanisms rely on perturbation periods of similar scale. We make use of the Bloch representation developed in the previous chapter to analyse both cases, and find the conditions for complete power transfer between two dissimilar cores in the grating assisted coupler.

5.2 The zero coupling condition

Consider the evanescent coupler with index modulated cores shown schematically in Fig. 5.1, where the darker shading corresponds to higher refractive index. In the central coupling region, the index modulations are exactly out of phase. The propagation constants $\beta_1(z)$ and $\beta_2(z)$ of the fundamental modes in cores 1 and 2, respectively, vary periodically with distance z along the coupler. If the index modulations of the two cores are given by $\pm\delta n \sin(\omega_m z)$, where $\delta n \ll 1$ is the modulation amplitude and ω_m the modulation frequency, then correct to first order in δn [9]

$$\beta_1(z) = \beta_0 + k\eta\delta n \sin(\omega_m z), \quad (5.1)$$

$$\beta_2(z) = \beta_0 - k\eta\delta n \sin(\omega_m z), \quad (5.2)$$

where β_0 is the unperturbed propagation constant of the fundamental modes of both cores, $k = 2\pi/\lambda$ is the wavenumber, λ is the source wavelength and η is the fraction of modal power propagating in the cores. Propagation along the coupler is assumed to satisfy the weak-guidance condition so that the fundamental mode fields Ψ_1 and Ψ_2 of cores 1 and 2, respectively, are solutions of the scalar wave equation [9]. Furthermore, the modulation is assumed to be sufficiently slow along the axis that the coupling to

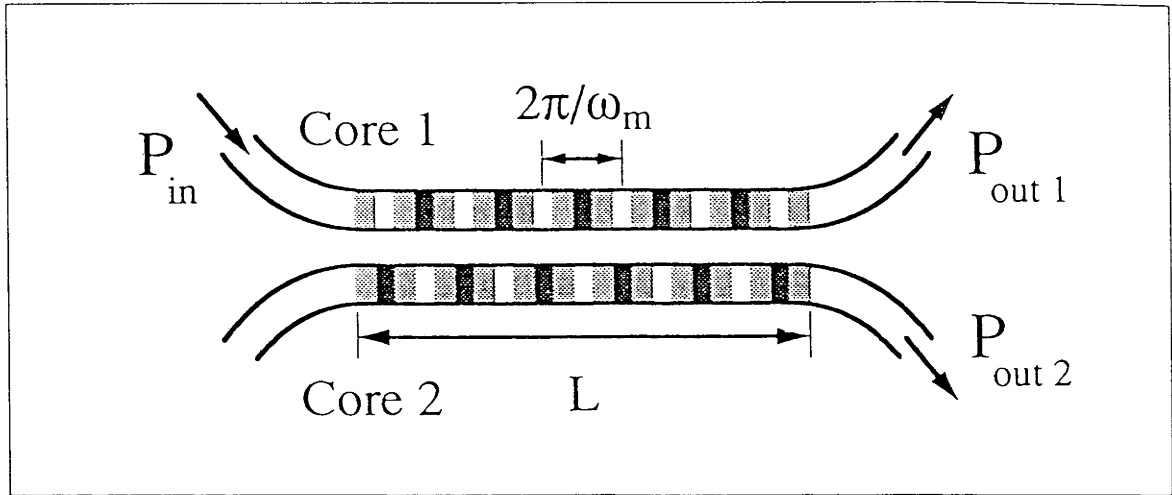


Figure 5.1: Schematic of a four-port modulated index coupler. Shadings represent out-of-phase periodic index modulations in each core. The length of the coupler is L and the index modulation period is given by $2\pi/\omega_m$.

higher-order leaky modes and backward-propagating modes is negligible. The respective amplitudes $a_1(z)$ and $a_2(z)$ of these fields satisfy the pair of lossless coupled-mode equations

$$\frac{da_1}{dz} - ik\eta\delta n \sin(\omega_m z)a_1 = iCa_2, \quad (5.3)$$

$$\frac{da_2}{dz} + ik\eta\delta n \sin(\omega_m z)a_2 = iCa_1, \quad (5.4)$$

where C is the coupling constant defined by

$$C = \frac{1}{4}k \left(\frac{\epsilon_0}{\mu_0} \right)^{1/2} \int_{A_{\text{co}1}} (n_{\text{cl}}^2 - n_{\text{co}}^2) \Psi_1 \Psi_2 dA. \quad (5.5)$$

Here n_{cl} is the uniform cladding index, n_{co} is the unperturbed core index and $A_{\text{co}1}$ denotes the cross-section of core 1. ϵ_0 and μ_0 are the electric permittivity and magnetic permeability of free space, respectively.

Although results from Fig. 5.2 are obtained from solving the coupled equations (5.3, 5.4) numerically, an accurate approximate solution for the zero coupling condition can be obtained by iteration. If we assume that light is launched into core 1 by setting $a_2 = 0$ in Eq. (5.3), then

$$a_1(z) = \exp \left\{ i \frac{k\eta\delta n}{\omega_m} [1 - \cos(\omega_m z)] \right\}, \quad (5.6)$$

assuming that $a_1 = 1$ at $z = 0$. On substituting Eq. (5.6) into Eq. (5.4), the small correction to $a_2(z)$ is given by

$$a_2(z) = iC \exp \left[\frac{-ik\eta\delta n(1 - \cos \omega_m z)}{\omega_m} \right] \int_0^z \exp \left[\frac{2ik\eta\delta n(1 - \cos \omega_m z)}{\omega_m} \right] dz. \quad (5.7)$$

so that $a_2 = 0$ at $z = 0$. Using standard formulae [7], the integral can be evaluated analytically as an infinite series. However, when z is an integral multiple m of the grating period, i.e. $z = 2\pi m/\omega_m$, the series reduces to the single term

$$a_2\left(\frac{2m\pi}{\omega_m}\right) = \frac{2m\pi i C}{\omega_m} J_0\left(\frac{2k\eta\delta n}{\omega_m}\right) \exp\left(\frac{2ik\eta\delta n}{\omega_m}\right), \quad (5.8)$$

Again we observe the familiar occurrence of the zeroth order Bessel function, J_0 . This result is valid provided that $\delta n \ll n_{co} - n_{cl}$ and the cores are sufficiently separated so that the modulation period is small compared with the coupling length, i.e. when $2\omega_m \gg C$. In this limit, the time step of $2\pi/\omega_m$ is sufficiently small so that at any time the assumption that a_2 is much smaller than a_1 is always true. Eq. (5.8) ensures that when

$$\frac{2k\eta\delta n}{\omega_m} = j_{0,m}, \quad (5.9)$$

where $j_{0,m}$ is the m th root of J_0 , the field amplitude in core 2 is always zero at all integer multiple distance of the modulation period. Hence, Equation (5.9) give us the zero coupling condition of the modulated index coupler. Since the condition involves the wavenumber k , we note that the suppression of coupling is only occurring at one wavelength.

5.3 Numerical results

The coupled mode Eqs. (5.3, 5.4) were solved numerically, and the power transfer, i.e., the fraction of power entering core 1 at $z = 0$ which exits core 2 is plotted in Fig. 5.2 as a function of the normalized distance z/L_C along the coupler, for a range of values of δn . In Fig. 5.2, curve (a) shows the familiar periodic power transfer between two identical cores ($\delta n = 0$). The remaining curves (b) - (d), illustrate how the applied index modulation affects the power transfer: in each case there is a small rapid power oscillation, (two cycles per index modulation period), superimposed on a complete sinusoidal power transfer over an effective length scale L_{eff} , longer than the standard coupling period L_C . Hence, the effective coupling constant $C_{\text{eff}} = \pi/L_{\text{eff}}$ decreases with δn . In curve (d) the accumulating power transfer is suppressed since δn satisfies Eq. (5.9) at the first root of J_0 . This corresponds to $C_{\text{eff}} \rightarrow 0$. Further increasing δn reintroduces power transfer between the cores, since $|J_0(2k\eta\delta n/\omega_m)| > 0$ again. The residual rapid power oscillation in Fig. 5.2d involves less than 2% of the total input power. Even smaller residues could be achieved by decreasing the modulation period, while increasing δn to maintain the zero coupling condition of Eq. (5.9).

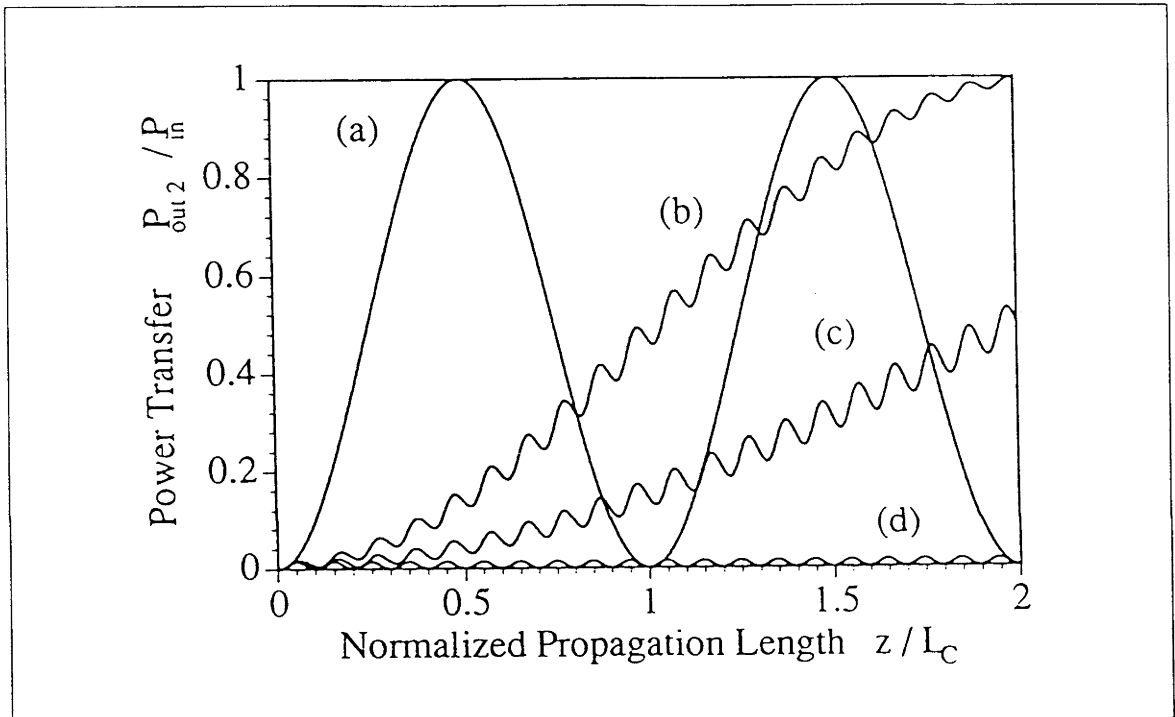


Figure 5.2: Power transfer of a four-port modulated index coupler

Normalized power transfer $P_{\text{out}2}/P_{\text{in}}$ in a four-port index modulated coupler operating at $1.3\mu\text{m}$, for various amounts of core index modulation $\delta n =$ (a) 0 , (b) 1.98×10^{-3} , (c) 2.20×10^{-3} and (d) 2.44×10^{-3} (the last case corresponding to $2k\eta\delta n/\omega_m = 2.405$, the first zero of J_0). Power transfer is plotted over two standard coupling lengths of the unmodulated coupler. Here the fractional modal power in the core $\eta = 0.750$, $L_C = 4.27\text{mm}$ is the coupling length, and the modulation period, $2\pi/\omega_m = 0.854\text{mm}$, (corresponding to $\omega_m = 10C$)

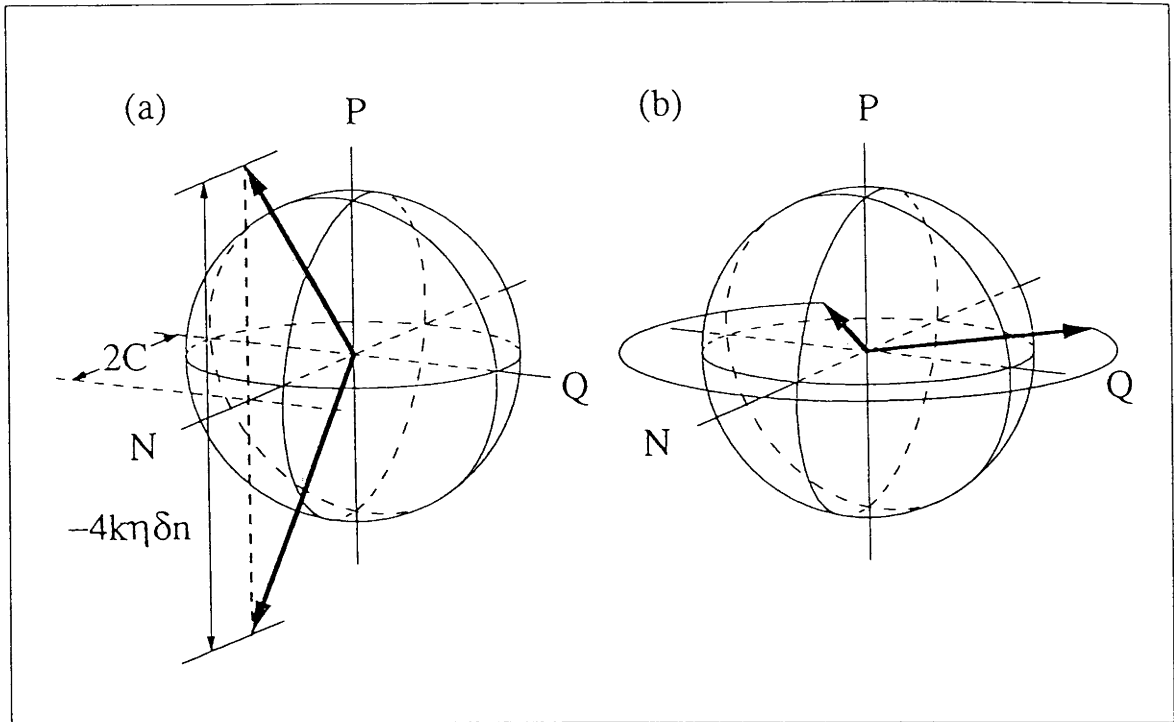


Figure 5.3: Bloch representation of a four-port modulated index coupler
 (a) In the rotating frame with constant frequency, the torque vector is given by $\vec{F} = (2C, 0, -2k\eta\delta n \sin(\omega_m z))$; (b) In the rotating frame with phase modulated frequency, the torque vector is given by $\vec{F} = (2C \cos[2k\eta\delta n \cos(\omega_m z)/\omega_m], 2C \sin[2k\eta\delta n \cos(\omega_m z)/\omega_m], 0)$

5.4 Bloch representation of the modulated index coupler

The coupled mode equations (5.3, 5.4) for the modulated index coupler which has been demonstrated to suppress coupling can be transformed into the Bloch sphere representation by the method discussed in Chapter 4. Using Eqs. (4.47, 4.48, 4.49) we obtain

$$\frac{dN}{dz} = 2k\eta\delta n \sin(\omega_m z)Q, \quad (5.10)$$

$$\frac{dQ}{dz} = -2k\eta\delta n \sin(\omega_m z)N - 2CP, \quad (5.11)$$

$$\frac{dP}{dz} = 2CQ. \quad (5.12)$$

The torque equation is hence given by

$$\vec{O} = (2C, 0, -2k\eta\delta n \sin(\omega_m z)) \times \vec{O}. \quad (5.13)$$

Having simplified the problem to three dimensions, we can now choose a suitable

rotating frame to aid our analysis further. Because we are mainly interested in the powers in both of the cores, i.e., in the P -axis, any rotation about the NQ -plane will not change the final results since the P -axis is invariant under the rotation. We choose a rotating frame which has a modulated rotating frequency to help us to decompose the index modulation into Fourier components. The new co-ordinates, denoted by primes, are given by,

$$\begin{pmatrix} N' \\ Q' \\ P' \end{pmatrix} = \begin{pmatrix} \cos \left[\frac{2k\eta\delta n}{\omega_m} \cos(\omega_m z) \right] & \sin \left[\frac{2k\eta\delta n}{\omega_m} \cos(\omega_m z) \right] & 0 \\ -\sin \left[\frac{2k\eta\delta n}{\omega_m} \cos(\omega_m z) \right] & \cos \left[\frac{2k\eta\delta n}{\omega_m} \cos(\omega_m z) \right] & 0 \\ 0 & 0 & 1 \end{pmatrix} \begin{pmatrix} N \\ Q \\ P \end{pmatrix}. \quad (5.14)$$

Equations (5.10, 5.11, 5.12) can now be written as,

$$\dot{N}' = -2C \sin \left[\frac{2k\eta\delta n}{\omega_m} \cos(\omega_m z) \right] P', \quad (5.15)$$

$$\dot{Q}' = -2C \cos \left[\frac{2k\eta\delta n}{\omega_m} \cos(\omega_m z) \right] P', \quad (5.16)$$

$$\dot{P}' = 2C \left\{ \cos \left[\frac{2k\eta\delta n}{\omega_m} \cos(\omega_m z) \right] Q' + \sin \left[\frac{2k\eta\delta n}{\omega_m} \cos(\omega_m z) \right] N' \right\}. \quad (5.17)$$

The torque equation after transformation is

$$\vec{\mathcal{O}} = \left(2C \cos \left[\frac{2k\eta\delta n}{\omega_m} \cos(\omega_m z) \right], 2C \sin \left[\frac{2k\eta\delta n}{\omega_m} \cos(\omega_m z) \right], 0 \right) \times \vec{\mathcal{O}}. \quad (5.18)$$

Fig (5.3) shows the torque vectors of the modulated index coupler in both the ordinary and phase modulated rotating frames. We can now perform a Fourier decomposition of the torque vector using standard formulae [7]

$$\begin{aligned} \vec{\mathcal{F}} = & \left(2C J_0 \left(\frac{2k\eta\delta n}{\omega_m} \right) + 4C \sum_{j=1}^{\infty} (-1)^j J_{2j} \left(\frac{2k\eta\delta n}{\omega_m} \right) \cos(2j\omega_m z), \right. \\ & \left. 4C \sum_{j=0}^{\infty} (-1)^j J_{2j+1} \left(\frac{2k\eta\delta n}{\omega_m} \right) \cos[(2j+1)\omega_m z], 0 \right) \end{aligned} \quad (5.19)$$

By assuming that the modulation period is much shorter than the coupling length, $2\omega_m \gg C$, we can make use of the rotating wave approximation and neglect the terms with oscillating frequency higher than the modulation frequency ω_m in the torque. This first order approximation to the torque now gives,

$$\vec{\mathcal{F}} = \left(2C J_0 \left(\frac{2k\eta\delta n}{\omega_m} \right), 0, 0 \right). \quad (5.20)$$

The Bloch representation analysis hence shows agreement with the result obtained from the iterative method. Furthermore, we now obtain a first order expression of the effective coupling constant:

$$C_{\text{eff}} = C \left| J_0 \left(\frac{2k\eta\delta n}{\omega_m} \right) \right|. \quad (5.21)$$

Hence when the argument of the zeroth order Bessel function takes the value of one of the roots, coupling between the cores is completely suppressed.

The second order effect of the periodic index modulation is obtained by including terms with a slightly faster rotation frequency of ω_m . The torque of the modulated index coupler is now given by

$$\vec{\mathcal{F}} = \left(2C J_0 \left(\frac{2k\eta\delta n}{\omega_m} \right), 4C J_1 \left(\frac{2k\eta\delta n}{\omega_m} \right) \cos(\omega_m z), 0 \right). \quad (5.22)$$

It is this second order term which gives rise to the power oscillation seen superimposed on the slower power transfer curve.

5.5 Square-wave longitudinal index coupler

Analysis of the modulated index coupler can be further simplified if we assume that the refractive indices are instantaneously flipping between two values at a regular time interval. Physically, such instantaneous changes in the refractive indices will give rise to backward propagating modes more readily than the case of the slow sinusoidal modulation of the refractive indices. We therefore only use this example as a theoretical tool for understanding the periodic undoing of phase accumulation.

We now suppose that the core indices vary with propagation length according to,

$$n_1(z) = \begin{cases} n_0 + \delta n & \frac{2n\pi}{\omega_m} < z < \frac{(2n+1)\pi}{\omega_m}, \\ n_0 - \delta n & \frac{(2n+1)\pi}{\omega_m} < z < \frac{(2(n+1))\pi}{\omega_m}, \end{cases} \quad (5.23)$$

$$n_2(z) = \begin{cases} n_0 - \delta n & \frac{2n\pi}{\omega_m} < z < \frac{(2n+1)\pi}{\omega_m}, \\ n_0 + \delta n & \frac{(2n+1)\pi}{\omega_m} < z < \frac{(2(n+1))\pi}{\omega_m}, \end{cases} \quad (5.24)$$

where n_0 is the average core index. The torque vector is now given by

$$\vec{\mathcal{F}} = \begin{cases} (2C, 0, 2k\eta\delta n) & \frac{2n\pi}{\omega_m} \leq z < \frac{(2n+1)\pi}{\omega_m}, \\ (2C, 0, -2k\eta\delta n) & \frac{(2n+1)\pi}{\omega_m} \leq z < \frac{2(n+1)\pi}{\omega_m}, \end{cases} \quad (5.25)$$

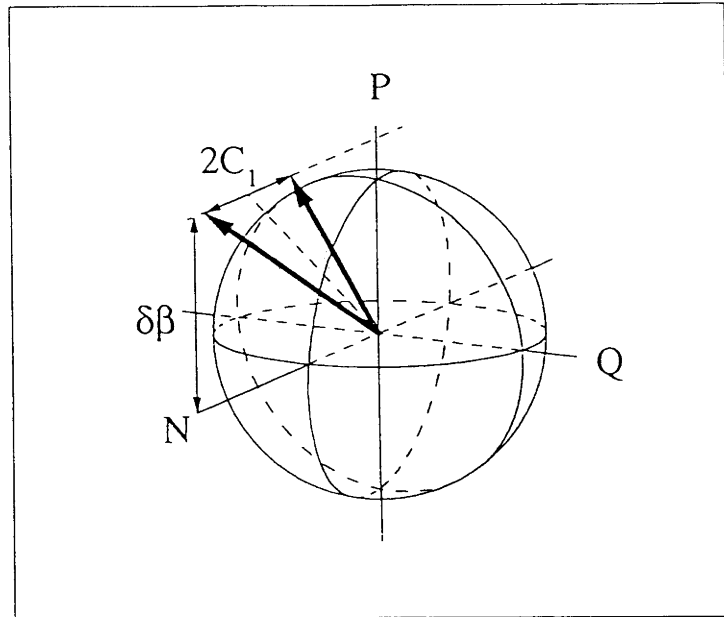


Figure 5.4: Bloch representation of the grating assisted coupler

since in any given length interval, the coupler is just a normal dissimilar core coupler. Notice that in this case, the torque vector has a constant length of

$$|\vec{\mathcal{F}}| = \sqrt{(2C)^2 + (2k\eta\delta n)^2}. \quad (5.26)$$

The evolution of the optical field vector can now be solved analytically for every time interval of constant torque. If we chose the modulation frequency so that it satisfies a periodicity condition, i.e.,

$$\omega_m = \sqrt{(2C)^2 + (2k\eta\delta n)^2}, \quad (5.27)$$

then at the end of every constant torque time interval, the optical field vector returns to its initial position. This illustrates the concept of the undoing of phase accumulation. If an initial state of $P = -1$ is assumed, the optical vector will describe a “figure 8” on the bottom of the Bloch sphere and the maximum power transfer experienced by the optical coupler in this case is simply

$$\left(\frac{P_{\text{out}2}}{P_{\text{in}}}\right)_{\text{max}} = \frac{4C^2}{4C^2 + (2k\eta\delta n)^2}. \quad (5.28)$$

Hence, if the coupling constant of the coupler is relatively small compared with the index change of δn , power transfer is negligible. Since the zero coupling condition involves the ratio of δn and ω_m , we can therefore conclude that maximum power transfer is negligible when $2\omega_m \gg C$.

5.6 Grating assisted coupler

In this section, we use the Bloch representation to analyse the grating assisted coupler. The coupled mode equations for the grating assisted coupler are given by,

$$\frac{da_1}{dz} = i\beta_1 a_1 + i(C_0 + C_1 \sin \omega_m z) a_2, \quad (5.29)$$

$$\frac{da_2}{dz} = i\beta_2 a_2 + i(C_0 + C_1 \sin \omega_m z) a_1, \quad (5.30)$$

where C_0 is the unperturbed coupling constant of the coupler; C_1 and ω_m are the grating amplitude and frequency. Rewriting these equations in terms of the N , Q and P parameters gives,

$$\frac{dN}{dz} = -\delta\beta Q, \quad (5.31)$$

$$\frac{dQ}{dz} = \delta\beta N - 2(C_0 + C_1 \sin \omega_m z) P, \quad (5.32)$$

$$\frac{dP}{dz} = 2(C_0 + C_1 \sin \omega_m z) Q, \quad (5.33)$$

where, $\delta\beta = \beta_2 - \beta_1$. Fig. 5.4 shows the torque representation of the grating assisted coupler. If we assume that the modulation of the coupling constant is small compared to the actual coupling, i.e., $C_1 \ll C_0$ so that

$$|\vec{\mathcal{F}}| \approx |\vec{\mathcal{F}}|_{\text{ave}} = \sqrt{(2C_0)^2 + (\delta\beta)^2}, \quad (5.34)$$

a periodicity condition which is necessary for inducing complete power transfer between dissimilar cores can be obtained. The periodicity condition is given by,

$$\omega_m = \sqrt{(2C_0)^2 + (\delta\beta)^2}. \quad (5.35)$$

To first order this periodicity condition ensures that the optical field vector is periodically returning to the initial starting value after each period of coupling modulation. However, the presence of the small modulation of the coupling constant induces an incremental climb of the optical field vector from the bottom pole of the sphere to the top pole as shown by numerical solutions of Eqs. (5.29, 5.30) in Fig. 5.5.

The other necessary condition for achieving complete power transfer is to require that the incremental climb be sufficiently small so that the optical field vector will not be passing through the top pole of the P -axis without approaching it close enough. This simply translates into having the modulation frequency sufficiently larger than the coupling constant. The results of this simple analysis using the Bloch representation

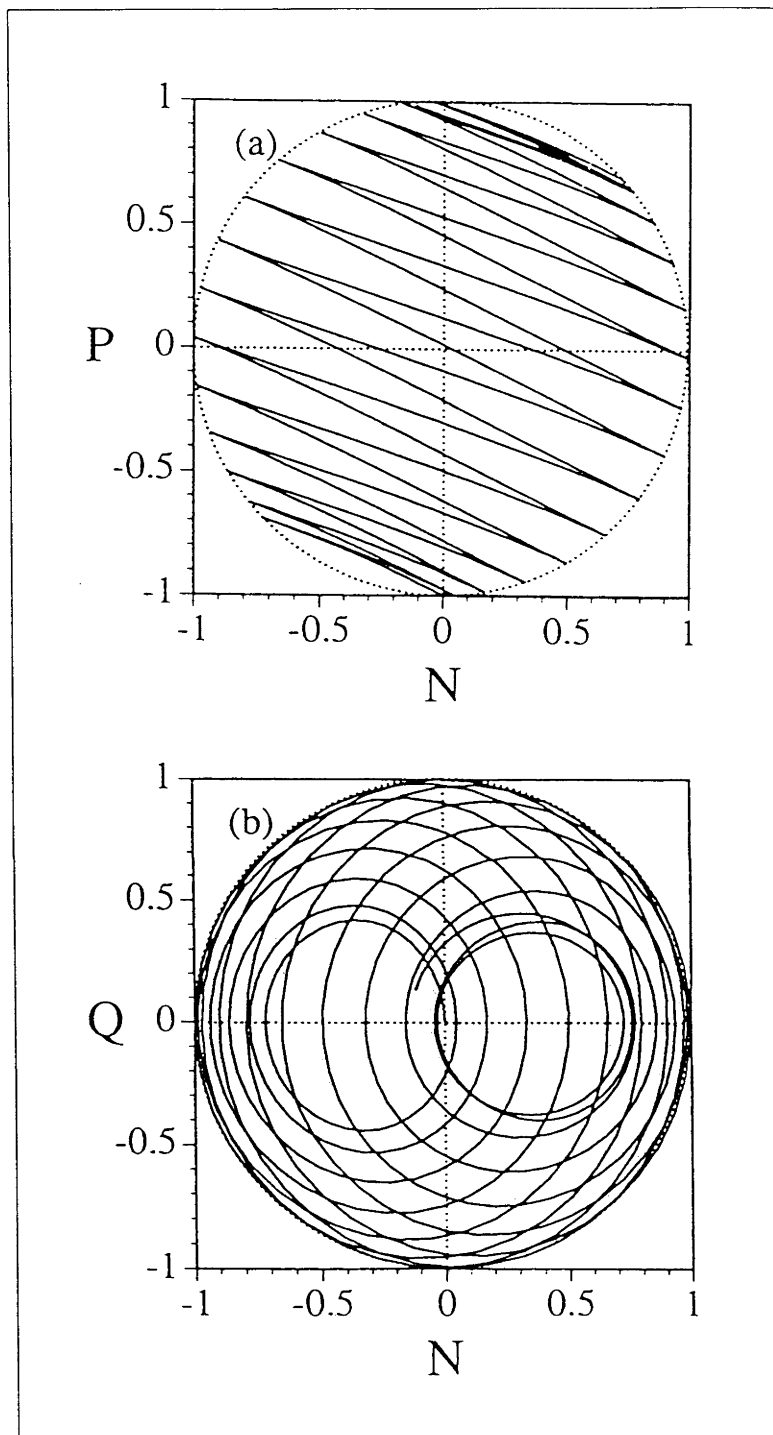


Figure 5.5: Optical field vector evolution of the grating assisted coupler
(a) P - N plot of the optical field vector; (b) Q - N plot of the optical field vector. Note that the optical field climbs incrementally from the bottom pole to the top pole of the P -axis. This corresponds to a complete power transfer which is normally not possible for dissimilar core couplers.

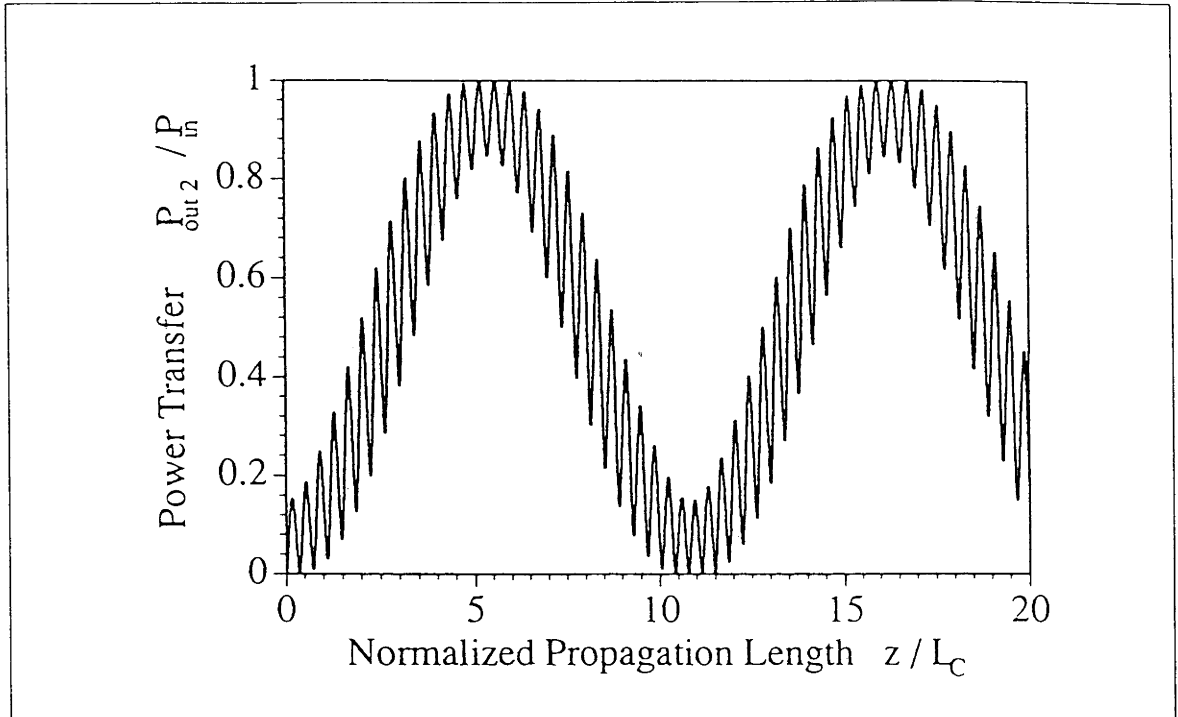


Figure 5.6: Power transfer of the grating assisted coupler

The normalized power transfer $P_{\text{out}2}/P_{\text{in}}$ of the grating assisted coupler versus normalized length. Complete power transfer is achieved after approximately $z = 5.5L_C$, where $L_C = \pi/C_0$.

of the coupler exactly agrees with the results stated by [16] in the limit when the cores of the coupler become very dissimilar,

$$(C_0 + C_1 \sin \omega_m z) \ll \delta\beta. \quad (5.36)$$

The conditions given were [16],

$$\omega_m = |\delta\beta|, \quad (5.37)$$

$$\omega_m \gg C_0. \quad (5.38)$$

Hence, the conditions obtained above Eqs. (5.35, 5.38) are a generalization of the complete power transfer conditions and are applicable even to the case when the cores of the coupler are slightly dissimilar.

5.7 Conclusion

In conclusion, we have demonstrated that an out-of-phase modulation of the refractive indices of coupler cores can control and completely suppress coupling. This is explained

in terms of the periodic undoing of the phase accumulation induced by the index modulation. We have also shown that the Bloch representation of the optical coupler is a useful tool for the visualization of the optical state in couplers. Using the Bloch representation, a more accurate condition for complete power transfer for the grating assisted coupler is obtained.

Chapter 6

Band-Pass Optical Coupler

6.1 Overview

Recently, two new schemes have been proposed for the fabrication of optical band-pass filters using four-port couplers. J. -L. Archambault et. al. [32] from the University of Southampton suggested the use of photorefractive Bragg gratings in optical couplers to achieve wavelength selectivity. Their proposed “grating frustrated coupler” is made up of an identical core coupler, with the Bragg gratings written along only one of the cores. When the light launched into the coupler is near the Bragg wavelength, the gratings introduce a strong dispersion, making the two cores asynchronous or phase mismatched; at the same time, they also create a barrier that rejects tunneling photons. This coupler was shown to achieve 70% peak transmission with a bandwidth of 0.7nm. Because of the Bragg reflection property, the required grating period is given by $\lambda_B = 2n_{\text{eff}}\Lambda$, where n_{eff} is the mode index and λ_B is the transmission wavelength. The index modulation period Λ is normally of the order of 500nm.

H. H. Yaffe et. al. [33] from AT&T Bell laboratories on the other hand, used multiple Mach-Zehnder sections to create a “resonant coupler”. Their filter was made with silicon-on-silicon waveguide technology, consisting of a series of parallel waveguide couplers connected by waveguides of unequal arm lengths (Mach-Zehnder interferometer) of the order of millimetres. Resonance is achieved by making the arm length difference the same for all pairs of arms. It was demonstrated that the peak transmission achieved has less than 1dB loss with a bandwidth of about $0.1\mu\text{m}$. The entire device length is hence about 30–40mm.

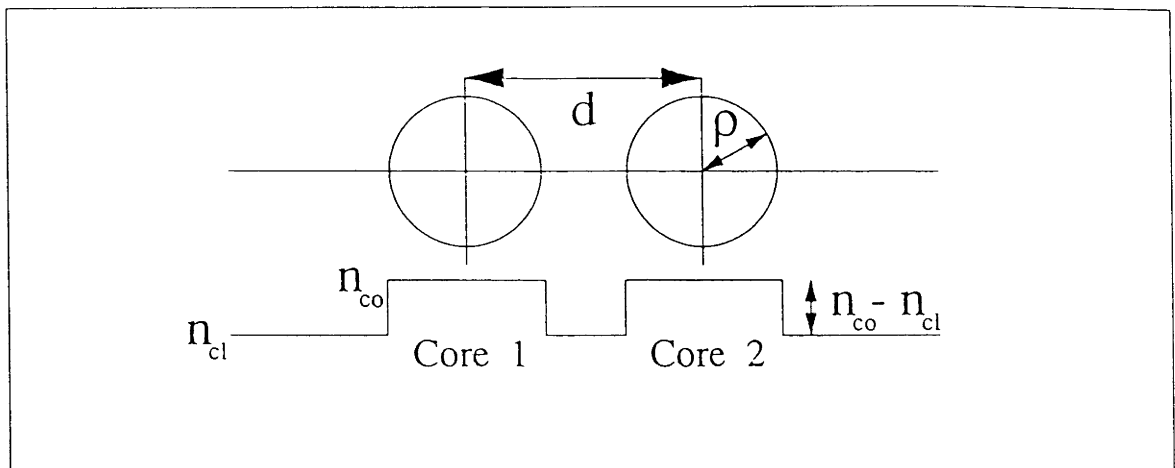


Figure 6.1: Twin fibre band-pass filter geometry

The radius of the fibres are given by ρ and the core to core separation is d . The lower half of the figure show the step-index profile of the coupler.

In this chapter, we demonstrate that the modulated index coupler also have band-pass filter characteristics, with the addition of an absorptive medium along one of its cores. Hence, this is an alternative mechanism to the existing two proposals. Our study shows that the modulation period required for the fabrication of such a band-pass filter is of the order of $100\mu\text{m}$, which is in between the two existing wavelength selective mechanisms. Theoretically, it was found that 50dB suppression of other wavelengths is achievable.

6.2 Wavelength dependence of the modulated index coupler

In order to work out the spectral response of a four-port modulated index coupler, we must first define the coupler geometry and from there obtain the coupler parameters as a function of wavelength. We assume that our modulated index coupler is made up of a pair of identical cylindrical fibres with the geometry shown in Fig. 6.1. The two cores are evanescently coupled and have a step-index profile. The coupling constant of a coupler, assuming weak-guidance, is given by [9]

$$C = \frac{1}{4}k \left(\frac{\epsilon_0}{\mu_0} \right)^{1/2} \int_{A_{\text{co}1}} (n_{\text{cl}}^2 - n_{\text{co}}^2) \Psi_1 \Psi_2 dA. \quad (6.1)$$

where $A_{\text{co}1}$ denotes the cross-section of core 1. Hence, $C \rightarrow 0$ with increasing core-to-core separation d . In the case of the geometry shown in Fig. 6.1, the coupling constant

is given by [9]

$$C = \frac{(2\Delta)^{1/2} U^2 K_0(Wd/\rho)}{\rho V^3 K_1^2(W)} \approx \left\{ \frac{\pi\Delta}{Wd\rho} \right\}^{1/2} \frac{U^2 \exp(-Wd/\rho)}{V^3 K_1^2(W)}, \quad (6.2)$$

where Δ is the profile height parameter, U is the core parameter, V is the waveguide parameter and W the cladding parameter. These parameters are given by

$$\begin{aligned} \Delta &= \frac{n_{co}^2 - n_{cl}^2}{2n_{co}^2} \\ &\approx \frac{n_{co} - n_{cl}}{n_{co}} \end{aligned} \quad (6.3)$$

$$U = \rho(k^2 n_{co}^2 - \beta^2)^{1/2} \quad (6.4)$$

$$\begin{aligned} V &= k\rho(n_{co}^2 - n_{cl}^2)^{1/2} \\ &\approx k\rho n_{co}(2\Delta)^{1/2} \end{aligned} \quad (6.5)$$

$$W = \rho(\beta^2 - k^2 n_{cl}^2)^{1/2} \quad (6.6)$$

The propagation constant of each fibre can be obtained using the equation [9]

$$U \frac{J_1(U)}{J_0(U)} = W \frac{K_1(W)}{K_0(W)}. \quad (6.7)$$

With these we can now obtain the fraction of modal power in each fibre using

$$\eta = \frac{U^2}{V^2} \left\{ \frac{W^2}{U^2} + \frac{K_0^2(W)}{K_1^2(W)} \right\} \quad (6.8)$$

These parameters are then substituted into the coupled mode equations (5.3, 5.4) and the equations are integrated to a fixed length for values of the wavenumber k from $1.2\mu\text{m}$ to $1.6\mu\text{m}$. Fig. 6.2 shows the plot of effective coupling constant C_{eff} versus wavelength for a twin fibre coupler with and without index modulation. The effective coupling constant of the coupler is defined as

$$C_{\text{eff}} = \frac{\pi}{L_{\text{eff}}}, \quad (6.9)$$

where L_{eff} is the period taken for a complete power transfer cycle. For an unmodulated coupler the coupling constant increases with wavelength monotonically. As predicted by earlier analysis, the modulated index coupler produces suppression of coupling at only one wavelength. In this case, the wavelength chosen to satisfy the zero coupling condition of Eq. (5.9) is $1.3\mu\text{m}$, which is the wavelength for most of the optical fibre communication application. Since to the first order the index modulation modifies the coupling constant by a factor of the modulus of the zeroth order Bessel function,

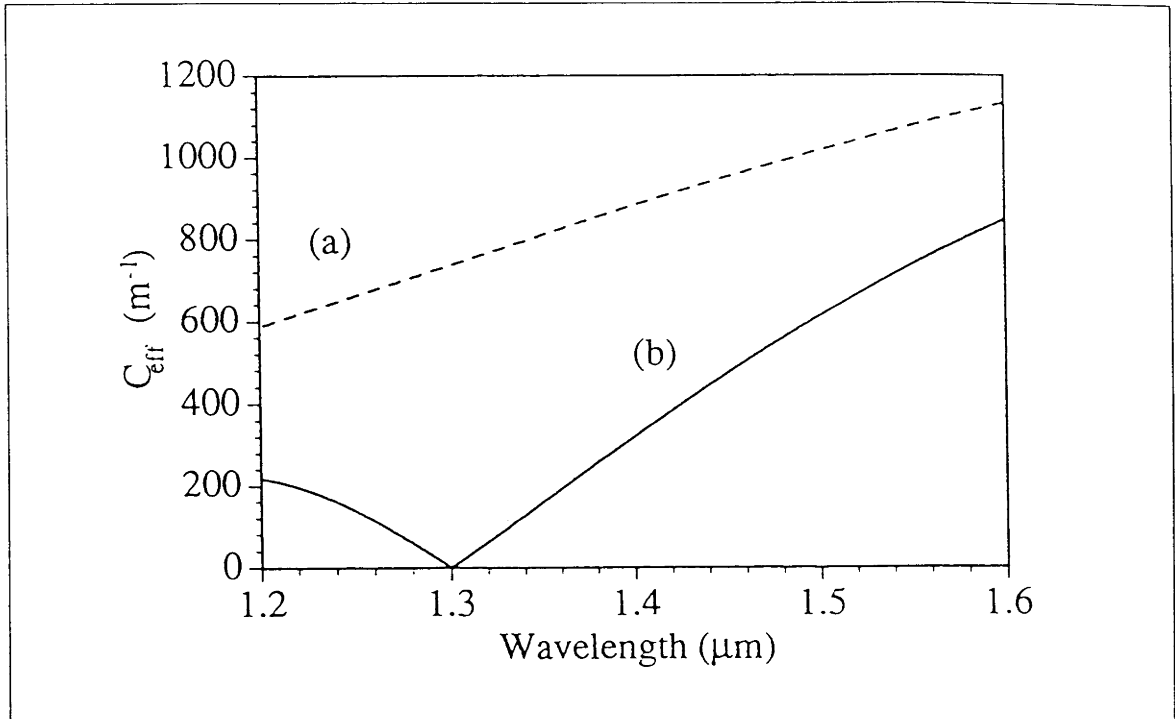


Figure 6.2: Effective coupling constant versus wavelength

The effective coupling constant versus wavelength of a four-port fibre coupler. Here, $\rho = 3.5\mu\text{m}$, $d = 10\mu\text{m}$, $n_{\text{co}} = 1.450$ and $n_{\text{cl}} = 1.445$. The profile height parameter is $\Delta = 3.44 \times 10^{-3}$. In curve (a), the coupler is unmodulated (normal coupler); in curve (b) an index modulation of 2.44×10^{-3} is applied satisfying the zero coupling condition at a wavelength of $1.3\mu\text{m}$.

$|J_0(2k\eta\delta n/\omega_m)|$, we observe that the coupling constant increases rather abruptly on either side of the suppression wavelength. This suggests that the index modulated coupler is capable of providing good wavelength selectivity for optical device fabrication.

6.3 Modulated index band-pass filter

The fact that coupling between fibres is suppressed at a single wavelength alone is not sufficient for the fabrication of an optical band-pass filter. The spectral response of the lossless modulated index coupler is shown in Fig. 6.3. In comparison with a normal coupler Fig. 6.4 (without index modulation) of the same length and geometry, we observe that in both cases power is transmitted through to the output port 1 at numerous other wavelengths.

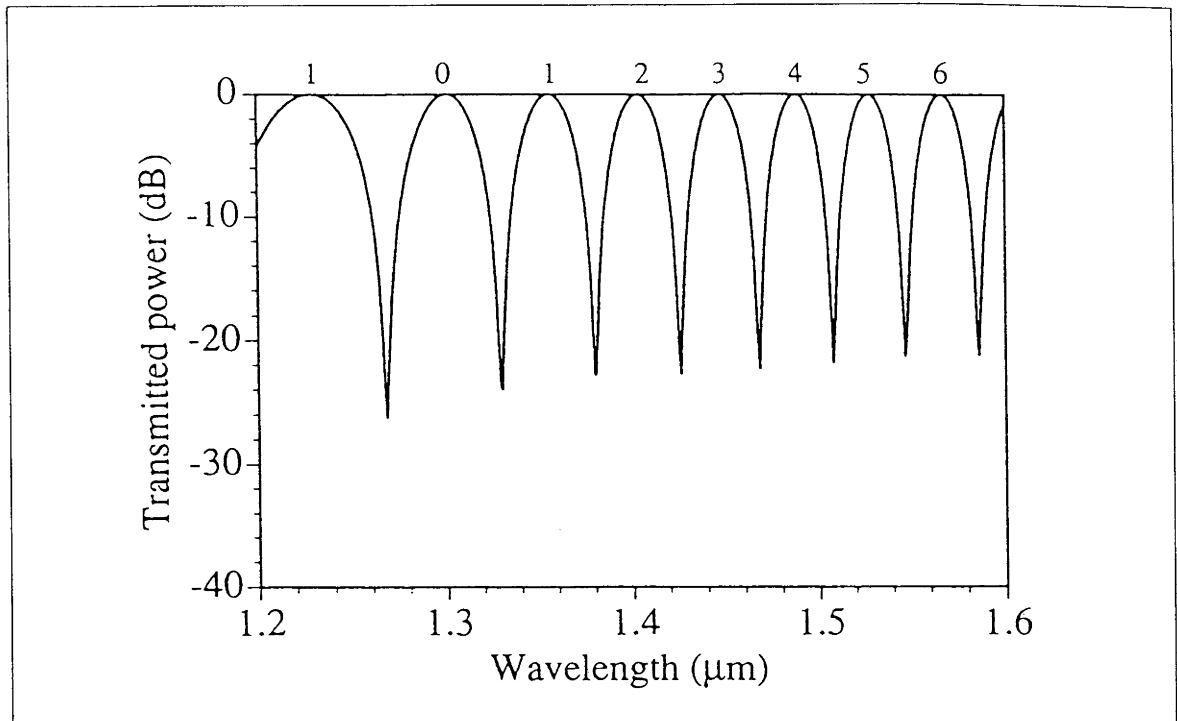


Figure 6.3: Spectral response of the four-port modulated index coupler. The numbers labeled on the transmission peaks are the number of complete power transfer cycles. The transmission peak at $1.3\mu\text{m}$ is due to suppression of coupling, hence it is labeled by the number zero. Here the coupler length is $L = 10C$.

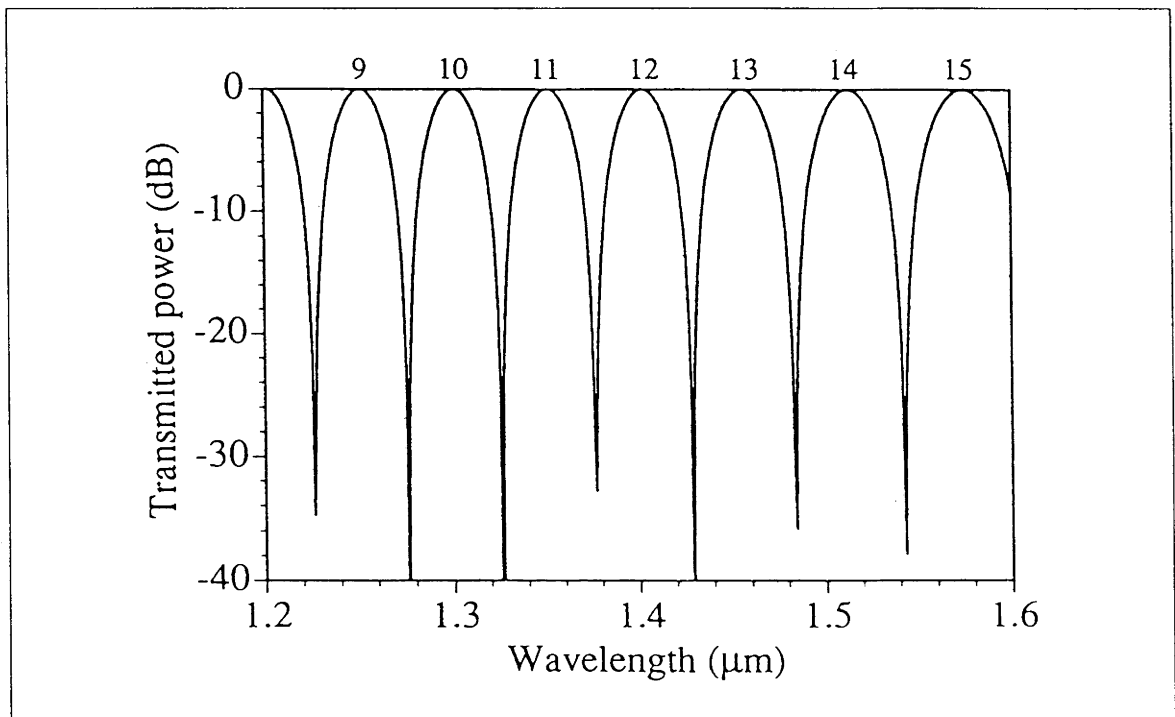


Figure 6.4: Spectral response of an identical core (unmodulated) coupler. Note that in this coupler although we still obtain a transmission peak at the wavelength of $1.3\mu\text{m}$, the light has actually gone through 10 complete power transfer cycles.

This is expected since for a fixed length coupler, some wavelengths would experience exactly an integral number of complete coupling cycles. Hence power at those wavelengths is being coupled back to the original fibre at the output port. The numbers labeled on the power transmission peaks of both Fig. 6.3 and Fig. 6.4 indicate the number of complete cycles the light of given wavelength has gone through before exiting at the output port of the coupler. Note that even when the chosen wavelength of $1.3\mu\text{m}$ experienced complete suppression of coupling, we have not yet observed any useful feature of the spectral response. Qualitatively, the only effect of coupling suppression is to spread out the spacings of the power transmission peaks.

We now add an absorptive medium along the second core of the coupler. This can be done, for example, by adding a metal strip along the outer side of the second core as shown in Fig. 6.5. We model this addition of absorptive metal by using the earlier coupled mode equations plus an additional absorptive term at the end of Eq. (5.4).

$$\frac{da_1}{dz} = ik\eta\delta n \sin(\omega_m z)a_1 + iCa_2, \quad (6.10)$$

$$\frac{da_2}{dz} = -ik\eta\delta n \sin(\omega_m z)a_2 + iCa_1 - \gamma a_2, \quad (6.11)$$

where γ is the decay constant of the absorptive medium. Since the metal strip is positioned at the outer side of the second core, the field amplitude of the first core is unaffected by it. If the coupling constant between the two cores is zero, the power of light launched into the second core would decay exponentially at the rate of $1/e^2$ for every unit length. Fig. 6.5 shows the schematic of the band-pass optical coupler and the metal strip absorber.

This band-pass filter makes use of the wavelength selective coupling suppression to suppress power transfer to the second core at only one wavelength. At this suppression wavelength, light in the first core is unaware of the presence of the additional absorptive medium in the second core and hence is transmitted through to the output port without any coupling to the second core in much the same way as before. For all other wavelengths, coupling is not completely suppressed, hence the power will eventually be transferred to the second core. Once the power begins to accumulate in the second core, the presence of the absorptive medium is felt and absorption of power occurs, preventing transmission of all other wavelengths, and thus forming the basis of a band-pass filter.

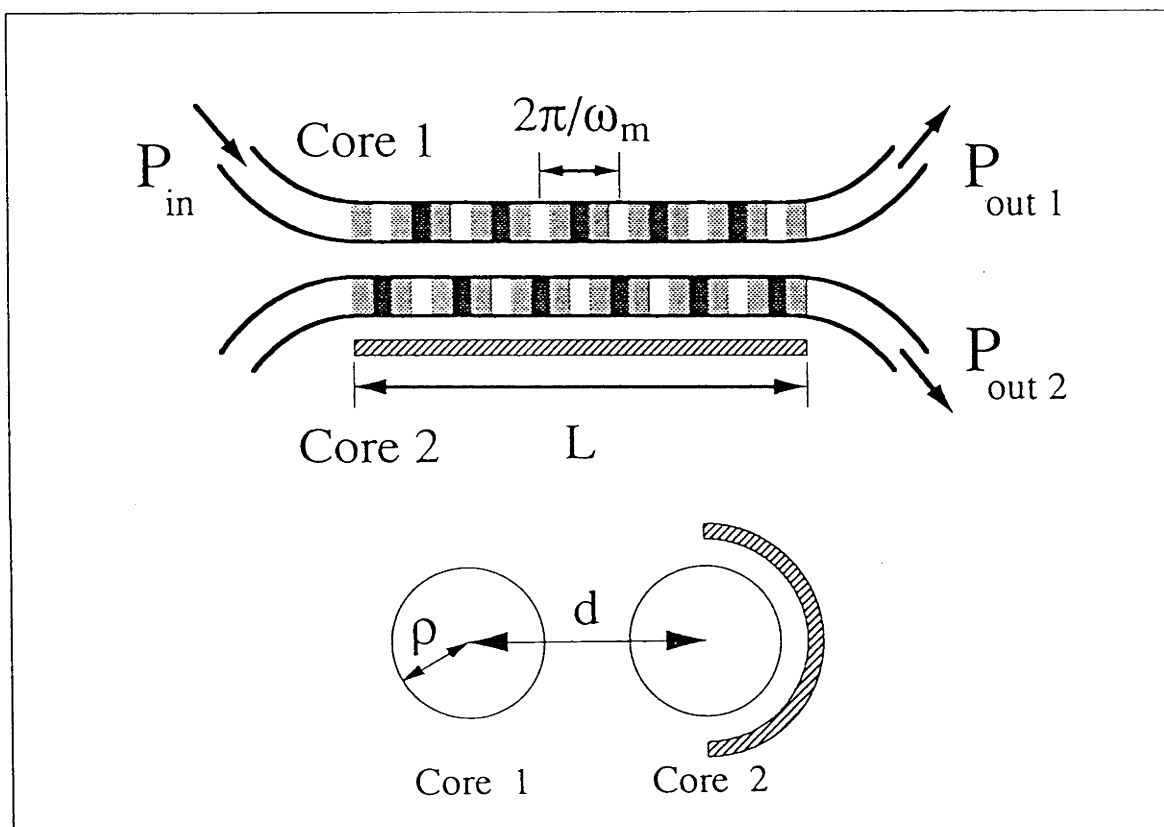


Figure 6.5: Schematic of the modulated index band-pass filter
The absorptive metal, represented by the striped area, is mounted on the outer side of the core 2 and light is launched into core 1.

6.4 Parameter variations

Fig. 6.6 shows the effect of varying the decay constant. Physically this corresponds to varying the metal strip to core separation. We observe that when the decay constant γ becomes non-zero, all transmission peaks except the suppression wavelength experience power loss. These peaks are called sidelobes and their heights decrease with increasing absorption. A suppression of more than 50dB is achievable for wavelengths above $1.4\mu\text{m}$ when $\gamma = 0.4C$. Increasing the decay constant increases the suppression level but also increases the bandwidth of the band-pass filter.

Fig. 6.7 shows the effect of varying the device length. In order to compensate for the broadening of the bandwidth by increasing the decay constant, we can increase the device length to reduce the bandwidth again since a longer coupler simply squeezes all the sidelobes nearer to the suppression peak.

The final parameter to consider is the modulation frequency of the band-pass filter. Since the zero coupling condition Eq. (5.9) is given by a ratio of the refractive index to modulation frequency, the performance of the band-pass filter is limited by the achievable index variation. A larger index modulation implies that the zero coupling condition will occur at a higher modulation frequency. Since the analysis of the zero coupling condition requires that $2\omega_m \gg C$, higher modulation frequency ensures that the effect of higher order sidebands are negligible and thus achieves better coupling suppression.

6.5 Conclusion

We have demonstrated that modulated index couplers with the addition of an absorptive medium in one core exhibit band-pass filter characteristics. The transmitted wavelength of the filter is simply the coupling suppressed wavelength which can be tuned by varying the ratio of the index modulation amplitude and period. By varying the amount of absorption, we can adjust the level of suppression of other wavelengths. Numerical results show that 50dB suppression is achievable for reasonable coupler parameters. Unlike normal wavelength division multiplexers, this new type of coupler is not critical to length variation. However, we can vary the length of the coupler to obtain different filter bandwidths. It has been demonstrated that the modulated index

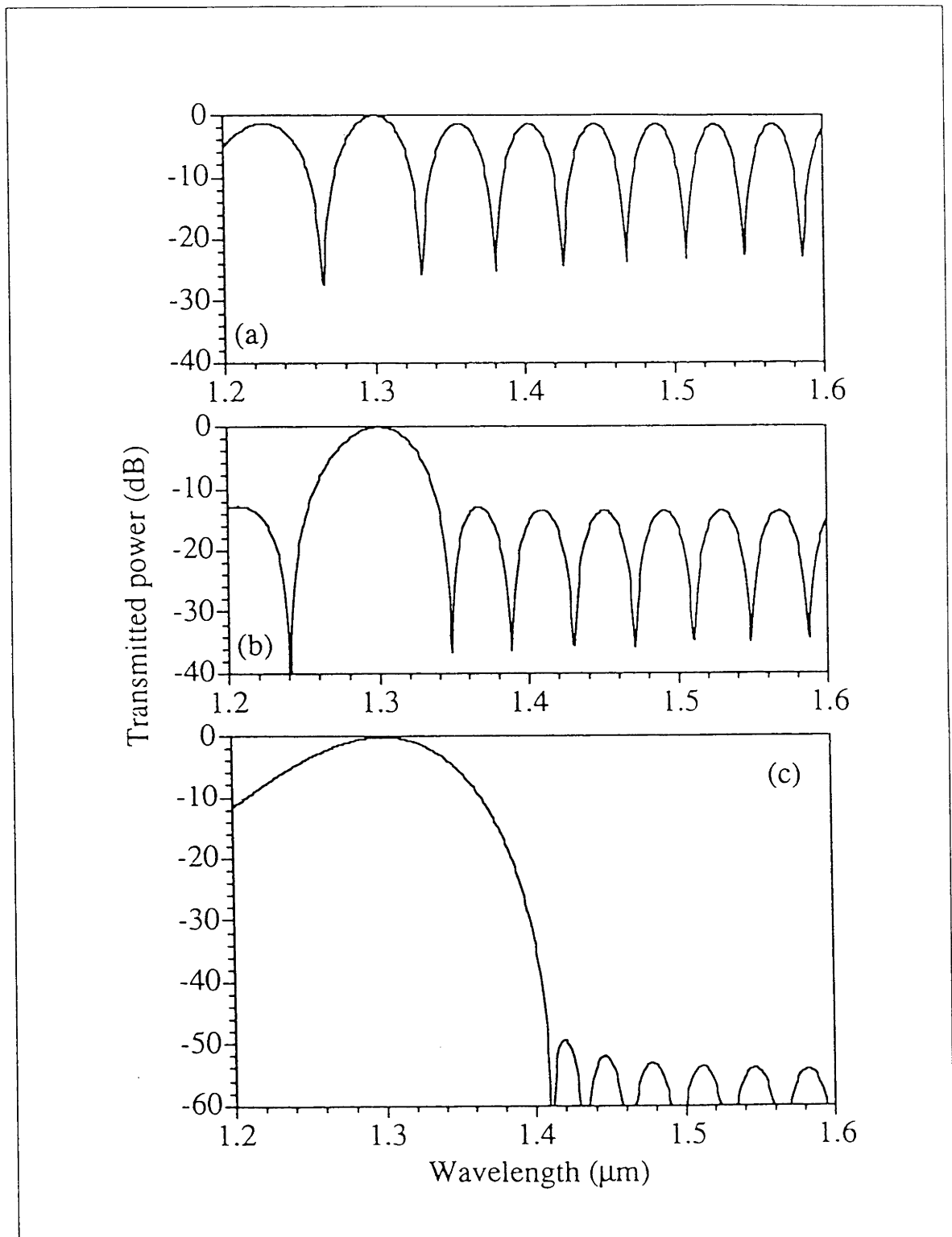


Figure 6.6: Effect of varying decay constant on band-pass filter response (a) $\gamma = 0.01C$, (b) $\gamma = 0.1C$ and (c) $\gamma = 0.4C$. Here the coupler length $L = 10C$ and the modulation frequency $\omega_m = 20C$. δn is chosen to satisfy the zero coupling condition at $1.3\mu\text{m}$.

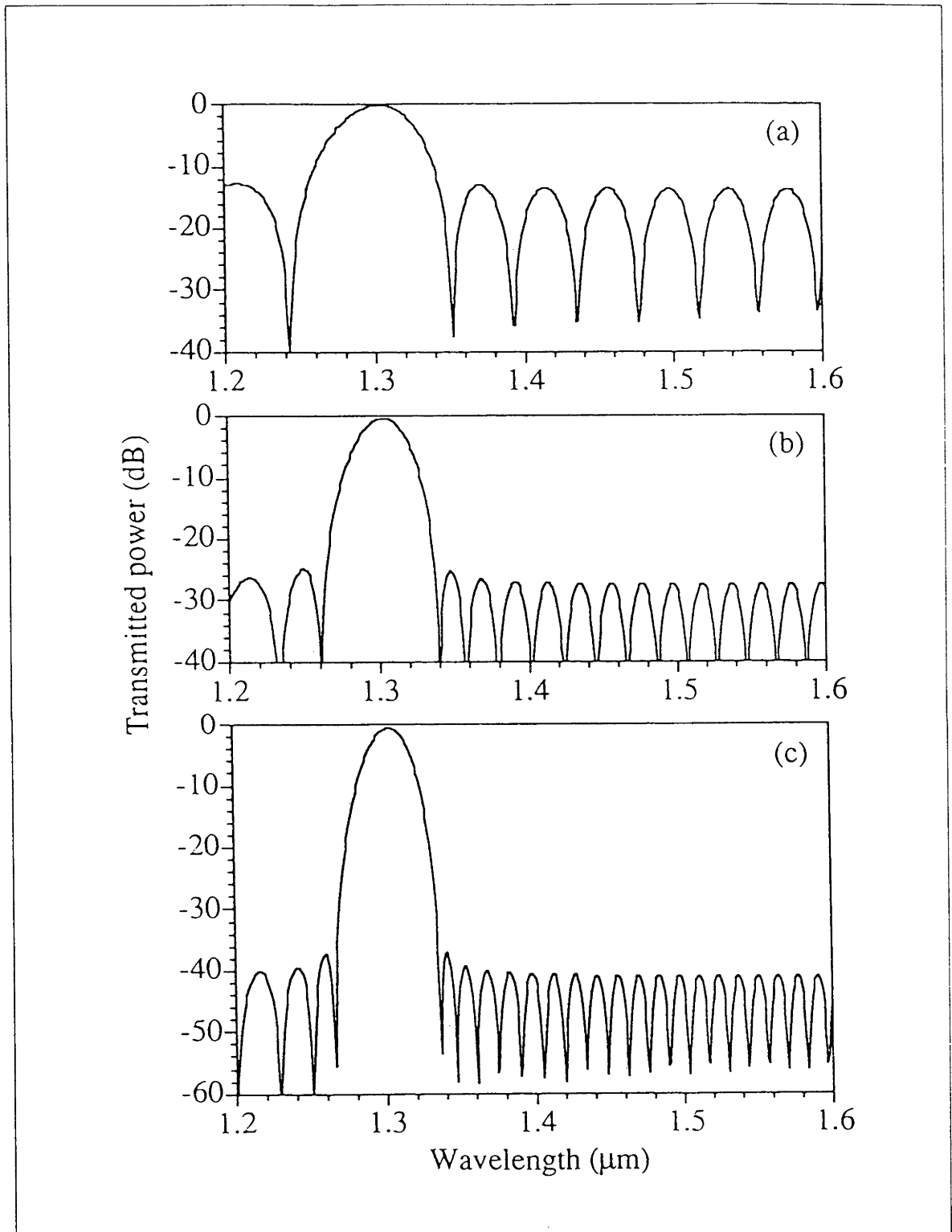


Figure 6.7: Effect of varying device length on band-pass filter response (a) $L = 10C$, (b) $L = 20C$ and (c) $L = 30C$. Here the decay constant $\gamma = 0.1C$ and the modulation frequency $\omega_m = 10C$. δn is chosen to satisfy the zero coupling condition at $1.3\mu\text{m}$.

coupler is a feasible alternative to the existing mechanisms of filter fabrication using Bragg gratings [32] or Mach-Zehnder sections [33]. Furthermore, since index modulation can be induced by the electro-optics effect, it gives the possibility of fabricating optical switches.

Chapter 7

Conclusion

In this thesis, we have studied the effect of periodic perturbations on two optical two-level systems: a two-level atom interacting with laser light and the optical state evolution of a single-mode optical coupler. The major results of this thesis are:

1. Complete atomic population inversion is shown to be achievable by interacting a two-level atom with light without any resonant frequency component. This phenomenon is called the correlated sideband inversion. Two examples of correlated sideband inversion are : phase modulated light with no resonant carrier and symmetrically detuned sidebands from amplitude modulated light.
2. It has been demonstrated that the presence of spontaneous emission does not destroy the effect of correlated sideband inversion. An optical experiment which can potentially observe the correlated sideband inversion is proposed.
3. We have related the work on the two-level atom to other works on the suppression of quantum tunneling. The analogy established between the two models allows us to explain the suppression of quantum tunneling in terms of sideband excitations. We have also extended the parameter regime for the generation of low-frequency radiation using the scheme proposed by Dakhnovskii and Metiu [31].
4. The Bloch representation for single-mode optical coupler is introduced. This new representation is demonstrated to be a convenient tool for visualizing the evolution of the optical state in a coupler.
5. Using the Bloch representation, we have obtained the conditions required for complete power transfer in the grating assisted coupler.

6. By introducing an out-of-phase periodic index modulation in the cores of a coupler, we have demonstrated that the power transfer between cores can be controlled and even totally suppressed.
7. The modulated index coupler can be used as an optical band-pass filter with the addition of an absorptive medium along one of the cores. The effects of varying coupler parameters on the filter response are studied.

Bibliography

- [1] J. C. Maxwell, Trans. R. Soc. CLV (1864).
- [2] L. Carol, "*Through the looking-glass and what Alice found there*" (1872).
- [3] F. Hund, Z. Phys. **43**, 803 (1927).
- [4] E. Kamke, "*Differentialgleichungen*", (Akademische Verlagsgesellschaft, Leipzig, 1945) pg.418, Eq. 2.66.
- [5] C. Cohen-Tannoudji and S. Haroche, J. de Physique **30**, 153 (1969).
- [6] D. T. Pegg and G. W. Series, "Semi-classical theory of the Hanle effect with transverse static and oscillating magnetic fields", J. Phys. B **3**, L33 (1970).
- [7] M. Abramowitz and I. Stegun, "*Handbook of Mathematical Functions*", (Dover, New York, 1972).
- [8] D. T. Pegg and G. W. Series, Proc. Roy. Soc. Lond. A **332**, 281 (1973).
- [9] A. W. Snyder and J. D. Love, "*Optical Waveguide Theory*" (Chapman & Hall, London, 1983).
- [10] J. J. Sakurai, "*Modern quantum mechanics*" (Addison-Wesley, 1985).
- [11] R. J. Black and A. Ankiewicz, "Fiber-optic analogies with mechanics", Am. J. Phys. **53**, 554 (1985).
- [12] A. M. Yariv, "*Optical Electronics*", (Holt-Saunders, New York, 1985).
- [13] L. Allen and J. H. Eberly, "*Optical Resonance and Two-Level Atoms*", (Dover, New York, 1987).
- [14] A. W. Snyder, A. Ankiewicz and A. Altintas, "Fundamental error of recent coupled mode formulations", Electronics Letts. **23**, 1097 (1987).

- [15] P. L. Chu and A. W. Snyder, "Theory of twin-core optical fibre frequency shifter", *Electronics Letts.* **23**, 1101 (1987).
- [16] D. Marcuse, "Directional Couplers Made of Nonidentical Asymmetric Slabs. Part II : Grating-Assisted Couplers", *IEEE J. Lightwave Tech.* **LT-5**, 268 (1987).
- [17] G. Meltz, W. W. Morey, and W. H. Glenn, "Formation of Bragg gratings in optical fibers by a transverse holographic method", *Opt. Lett.* **14**, 823 (1989).
- [18] W. -P. Huang and H. A. Haus, "Power Exchange in Grating-Assisted Couplers", *IEEE J. Lightwave Tech.* **7**, 920 (1989).
- [19] A. W. Snyder, Y. Chen and A. Ankiewicz, "Coupled Waves on optical fibers by power conservation", *J. Lightwave Tech.*, **7**, 1400 (1989).
- [20] W. A. Lin and L. E. Ballentine, "Quantum tunneling and chaos in a driven anharmonic oscillator", *Phys. Rev. Lett.* **65**, 2927 (1990).
- [21] W. W. Morey, "Tunable narrow-line bandpass filter" *Optical Fibre Communications Conference, Post-deadline paper, PD20-1* (1991)
- [22] P. Meystre and M. Sargent III, "*Elements of Quantum Optics*", (Springer-Verlag, New York, 1991).
- [23] Y. Chen and A. W. Snyder, "Grating-assisted couplers", *Opt. Lett.*, **16**, 217 (1991).
- [24] F. Großmann, P. Jung, T. Dittrich and P. Hanggi, "Tunneling in a periodically driven bistable system", *Z. Phys. B* **84**, 315 (1991).
- [25] F. Grossmann, T. Dittrich, P. Jung and P. Hanggi, "Coherent destruction of tunneling", *Phys. Rev. Lett.* **67**, 516 (1991).
- [26] R. Bavli and H. Metiu, "Laser-induced localization of an electron in a double-well quantum structure", *Phys. Rev. Lett.* **69**, 1986 (1992).
- [27] M. Andrews, P. M. Alsing, and C. M. Savage, "Comment on 'Coherent Destruction of Tunneling' ", unpublished (1992).
- [28] J. M. Gomez Llorente and J. Plata, "Tunneling control in a two-level system", *Phys. Rev. A*, **45**, R6958 (1992).

- [29] R. Kashyap, G. D. Maxwell, B. J. Ainslie, "Laser-trimmed four-port band-pass filter fabricated in singlemode photosensitive Ge-doped planar waveguide", *IEEE Photonics Tech. Lett.*, **5**, 191 (1993).
- [30] J. Plata and J. M. Gomez Llorente, "Control of tunneling in an electromagnetic cavity", *Phys. Rev. A* **48**, 782 (1993).
- [31] Y. Dakhnovskii and H. Metiu, "Conditions leading to intense low-frequency generation and strong localization in two-level systems", *Phys. Rev. A* **48**, 2342 (1993).
- [32] J. -L. Archambault et. al., "Grating-frustrated coupler: a novel channel-dropping filter in single-mode optical fiber", *Opt. Lett.*, **19**, 180 (1994).
- [33] H. H. Yaffe, C. H. Henry, M. R. Serbin and L. G. Cohen, "Resonant couplers acting as add-drop filters made with Silica-on-Silicon waveguide technology", *J. Light-wave Technol.*, **12**, 1010 (1994).
- [34] P. K. Lam and C. M. Savage, "Complete Atomic Population Inversion Using Correlated Sidebands", *Phys. Rev. A* **50**, 3500 (1994).
- [35] P. K. Lam, A. J. Stevenson and J. D. Love, "Coupling suppression by periodic index modulation in single-mode couplers" 19th Australian Conference on Optical Fibre Technology conference proceedings, Melbourne (1994).
- [36] Girish S. Agarwal and W. Harshawardhan, "Realization of trapping in a two-level system with frequency-modulated fields", *Phys. Rev. A* **50**, R4465 (1995).
- [37] P. K. Lam, A. J. Stevenson and J. D. Love, "Control and suppression of power transfer in couplers by periodic index modulation", *Electronics Letts.* **31**, 1233 (1995).